Journal of Bionic Engineering (2024) 21:1621–1643
https://doi.org/10.1007/s42235-024-00521-7

REVIEW ARTICLE

Research Progress on Bio-inspired Flapping-Wing Rotor Micro Aerial Vehicle Development

Yingjun Pan[1] · **Shijun Guo**[1] · **Xun Huang**[1]

Received: 8 July 2023 / Revised: 27 March 2024 / Accepted: 31 March 2024 / Published online: 12 July 2024
© The Author(s) 2024

Abstract

Flapping-wing rotor (FWR) is an innovative bio-inspired micro aerial vehicle capable of vertical take-off and landing. This unique design combines active flapping motion and passive wing rotation around a vertical central shaft to enhance aerodynamic performance. The research on FWR, though relatively new, has contributed to 6% of core journal publications in the micro aerial vehicle field over the past two decades. This paper presents the first comprehensive review of FWR, analysing the current state of the art, key advances, challenges, and future research directions. The review highlights FWR's distinctive kinematics and aerodynamic superiority compared to traditional flapping wings, fixed wings, and rotary wings, discussing recent breakthroughs in efficient, passive wing pitching and asymmetric stroke amplitude for lift enhancement. Recent experiments and remote-controlled take-off and hovering tests of single and dual-motor FWR models have showcased their effectiveness. The review compares FWR flight performance with well-developed insect-like flapping-wing micro aerial vehicles as the technology readiness level progresses from laboratory to outdoor flight testing, advancing from the initial flight of a 2.6 g prototype to the current free flight of a 60-gram model. The review also presents ongoing research in bionic flexible wing structures, flight stability and control, and transitioning between hovering and cruise flight modes for an FWR, setting the stage for potential applications.

Keywords Flapping-wing rotor · Micro aerial vehicle · Bio-inspiration · Flight

List of Symbols

MAV	= Micro aerial vehicle
FWR, FW, RW	= Flapping-wing rotor, flapping-wing, rotary-wing
VFW, HFW	= Vertical flapping-wing, horizontal flapping-wing
VTOL	= Vertical take-off and landing
AoA	= Angle of attack
LEV, TEV	= Leading edge vortex, trailing edge vortex
PPAV	= Passive pitching angle variation
Re, St	= Reynold number, Strouhal number
ρ	= Air density
$R_2, \bar{c}, S$	= Radius of the second area moment, mean chord, wing area
P_f	= Power factor
$t, \hat{t}, \hat{t}_r$	= Real time, non-dimensional time and reversal time interval
ψ, ϕ, α	= Rotation angle, flapping angle, pitching angle
$\dot{\phi}, \dot{\alpha}, \boldsymbol{\omega}$	= Flapping and pitching velocities, angular velocity vector
ψ_0, η	= Horizontal rotation speed, non-dimensional rotation speed
f, Φ, U	= Flapping frequency and amplitude, reference flapping velocity
α_u, α_d	= Geometric AoA at mid-upstroke and mid-downstroke
$\alpha_0, \Delta\alpha, \alpha_e$	= Mean AoA, pitching amplitude, the effective AoA
C_L, C_M, C_p	= Lift, rotational moment, and aerodynamic power coefficients
$\bar{C}_L, \bar{C}_M, \bar{C}_p$	= Average values of coefficients

✉ Yingjun Pan
y.pan@cranfield.ac.uk

Shijun Guo
sjguo368@gmail.com

Xun Huang
xun.huang@cranfield.ac.uk

[1] Centre for Aeronautics, School of Aerospace, Transport and Manufacturing, Cranfield University, Bedford MK43 0AL, UK

1 Introduction

The natural world, encompassing aquatic, terrestrial, and aerial fauna, serves as a rich source of inspiration for innovative robotic designs applicable across various scenarios and environmental conditions. Examples include the development of a cable-driven soft robot arm inspired by octopus tentacles for dynamic manipulation [1], a salamander-mimetic soft legged robot with capabilities for walking, crawling, rocking, and rolling suitable for diverse ground tasks [2], a hybrid aerial-aquatic flapping-wing microrobot [3], and a hybrid aerial-wall robotic insect [4]. Micro Aerial Vehicles (MAVs), which are ideally adapted for executing aerial intelligence, surveillance, and reconnaissance inside buildings and confined spaces, have attracted significant interest from both military and civilian end users in the past decades [5, 6].

MAVs are typically classified into fixed-wing, rotary-wing (RW), and flapping-wing (FW) types. Fixed-wing MAVs have advantages in aerodynamic efficiency and endurance on cruise, but lack the capability for vertical take-off and landing (VTOL) and hovering. Their performance significantly diminishes at very low Reynolds numbers. In contrast, RW MAVs are capable of VTOL, but their aerodynamic efficiency also suffers greatly at low Reynolds numbers. Furthermore, RW MAVs are not considered biomimetic, or inspired by biological models.

Flapping wings, inspired by the adept flying capabilities of natural fliers, present potential for mimicking the exceptional aerodynamic maneuvers observed in nature. Such wings are especially advantageous due to their lift mechanisms at low Reynolds numbers, making them suitable for miniaturization and compact applications of MAVs [7]. FW MAVs have a lower power demand in level flight compared to a fixed-wing MAV that often adapts a vertical propulsion system [8]. An insect-like FW MAV can produce lift in hover more efficiently with less power compared to a similar-size RW [9, 10]. In the past few years, the development of an FW MAV capable of VTOL and hovering has been motivated by scientific founding, along with commercial and military applications. The hummingbird-like aerial vehicle developed by Defence Advanced Research Project Agency in 2011 shows an encouraging example [11]. Except for unobtrusive surveillance in the security domain (such as police, defense, and special forces), scientists and robotic engineers have recently been fascinated by exploring diverse potential applications of biomimetic FW MAVs. These include aiding in insect or artificial pollination to enhance crop yields [12], as well as supporting special production needs in movies, performances, and documentary projects like BBC Spy in the Wild.

The pursuit of insect-inspired FW MAVs that can perform agile maneuvers and hover in both indoor and outdoor environments represents a promising direction for future applications. However, these current models face significant challenges, notably in achieving prolonged flight endurance. This limitation stems chiefly from the insufficient aerodynamic efficiency inherent in their design and the constraints of their power sources. Engineering these insect-like MAVs introduces unique challenges, particularly in the field of attitude control and stability, which diverge markedly from the control mechanisms observed in bird-like FW MAVs. Bird-like FW MAVs utilize their tails for attitude control, whereas insect-like FW MAVs delicately modulate wing kinematics, such as stroke amplitude, flapping speed, Angle of Attack (AoA), and stroke-plane deviation. Most insect-like MAVs are tailless and rely on flapping wings to produce control forces, resulting in agile flight maneuvers with more degrees of freedom [13, 14]. Furthermore, akin to soft robotics [1, 2], these bio-inspired flapping mechanisms engage in a complex interaction of rigid and flexible elements. The vibrations from flapping motions, coupled with the challenges of fluid–structure interactions due to wing flexibility, significantly complicate control systems.

For enhanced the aerodynamic efficiency of FW MAVs, a novel Flapping-Wing Rotor (FWR) combining bio-inspired FW and RW characteristics has been proposed. This compound biological configuration harnesses the advantages of multiple kinematics of flapping and rotation motions and is capable of VTOL and hovering. In 2003, Vandenberghe et al. [15] observed from their experiments that vertical flapping motion of wings generated thrust and imparted horizontal rotation to the wings. In 2007, Brandon [16] at the University of Maryland constructed a metal torqueless flapping rotor for MAVs, named 'Flotor', capable of producing lift and thrust akin to those produced by flying animals. This mechanism featured actively flapping wings driven by a motor and rotating passively. However, prior to Guo et al.'s proposal of the FWR concept in 2009 [17], the emphasis of these studies was on the physical phenomenon of flapping blades generating thrust, with minimal attention given to the contribution of wing flapping and rotation to lift enhancement for FW MAVs.

Guo et al. [17] demonstrated the feasibility of the FWR concept using a 9-gram prototype with compliant joints, driven by a piezoelectric actuator. Their experiments showcased the potential for power efficiency by utilizing system resonance and aeroelastic effects. In 2012, Guo and Li [18] made further experimental and numerical studies based on an enlarged piezoelectric actuated FWR. This study furnished valuable experimental data to corroborate theoretical and numerical models, thereby offering an effective

approach for designing FWRs, particularly in the computation of unsteady aerodynamic forces.

Piezoelectric actuators have high frequency and power density but inherently small amplitude, requiring a mechanical amplifier to achieve the necessary large amplitude for flapping wings. Thus, piezoelectric actuation is better suited for small-scale models. However, the high voltage power required by piezoelectric actuators is a practical barrier to their use in MAVs. Currently, a micro DC motor is the most practical option for the development of FWR MAVs. In 2011 and 2012, Li [19] and Wu [20] developed a 9.1 g and an 8.4 g FWR model, respectively, driven by an electric motor and simple crank-slider mechanism for lift measurement and feasibility evaluation. Guo et al. [21] manufactured and tested a flyable 2.6 g FWR model and achieved the first vertical take-off flight in 2014, which is the lightest flyable FWR model so far. Later in 2020, Dong et al. [22] built a 34 g FWR MAV and achieved free flight, making it the first flying FWR model with an onboard power and control system. Si et al. [23] performed a tethered take-off of an 18.7 g FWR model to demonstrate the effectiveness of passive pitching in 2021.

Over the past decade, a small number of researchers have dedicated their efforts to investigating FWR technology, comprising around 6% of publications in core journals within the MAV flied as depicted in Fig. 1. These investigation have predominantly centered on aerodynamic analysis and experimental assessments, significantly accelerating the progress in FWR development.

In this paper, we provide a comprehensive and up-to-date review of the progress made in the research of FWR MAVs and discusses the forthcoming challenges that need to be addressed for further advancements. We begin by introducing the novel FWR concept and the wing motions, followed by an overview of aerodynamics simulation and experimental measurement in Sect. 2.1. Our review highlights the FWR unique kinematics of motion and aerodynamic superiority over the traditional insect-like FW and RW. We also cover the latest achievements in lift enhancement through the optimization of wing geometric parameters, FWR kinematics of motion, such as asymmetrical upstroke and downstroke amplitudes and passive pitching, and elastic FWR mechanism in Sect. 2.2. We discuss the distinctive aerodynamic performance of FWR in both hovering and forward flight, influenced by different wing kinematics, in Sect. 2.3. Next, we focus on the mechanical system (in Sect. 3.1) and flight capabilities of FWR MAVs and compare them with existing flyable insect-like FW MAVs (in Sect. 3.2). We present recent progress in significantly increasing FWR aerodynamic lift and efficiency, which has enabled us to achieve VTOL flight from an FWR MAV of 20 g driven by a single motor to 60 g driven by double motors. In Sect. 4, we discuss the challenges and ongoing research in bionic flexible wing structure, VTOL stability and control, and transition from hovering to cruise flight mode of an FWR MAV to pave the way towards potential application. Finally, a conclusion of FWR research and development is presented in Sect. 5.

2 Aerodynamic Performance of FWR

2.1 FWR Kinematics of Motion

2.1.1 Wing Kinematics Definition

The readily observed flapping flight of birds and insects produces lift and thrust simultaneously, but their kinematics of flapping motion can be quite different. Most birds, except for small birds like hummingbirds, flap their wings in a nearly vertical stroke plane with a relatively low frequency and asymmetric up and downstrokes during cruise flight [24, 25]. In contrast, most insects flap their wings in a nearly horizontal stroke plane with a higher frequency and symmetric fore and back strokes during hovering, while most birds are

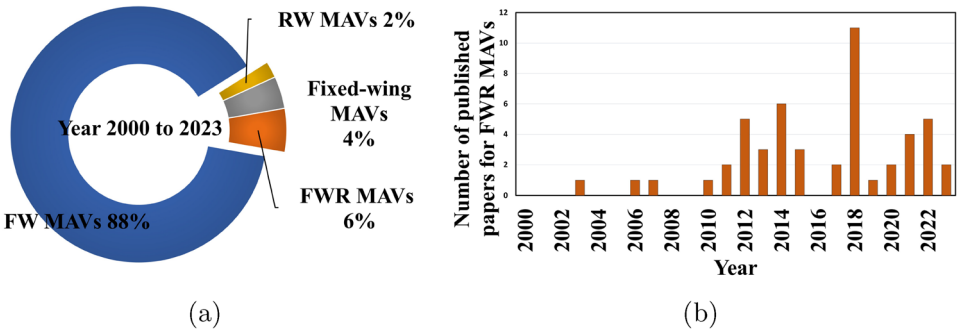

Fig. 1 **a** Publications on MAVs during the period from 2000 to 2023 (Data were taken from the Scopus database using search keyword: TITLE (flapping-wing AND robot OR vehicle OR MAV) for FW MAVs, TITLE (fixed-wing MAV) for fixed-wing MAVs, TITLE (rotary-wing OR rotorcraft AND MAV) for RW MAVs, respectively using (TITLE (flapping-wing rotor), TITLE (flapping-rotary wing) and TITLE (flapping perturbed revolving wing) for FWR MAVs). **b** Number of papers published on FWR MAVs each year

incapable. As insects fly forward, their stroke plane becomes more inclined forward [26].

As illustrated in Fig. 2a, a pair of insect wings arranged symmetrically about the x-axis produces lift in the y-axis and also thrust in the x-axis for forward flight [28, 29]. By reversing one of the wings in the opposite direction, the pair of wings becomes axially symmetric about the vertical y-axis or an asymmetrical arrangement about the x-axis like a rotary wing, as illustrated in Fig. 2b. The flapping wings still generate lift in the y-axis, but the associated thrust from the two wings generates a torque about the y-axis instead of a force in the same direction. When the wings are driven only in flapping motion (upstroke and downstroke), thrust will propel themselves to rotate due to the torque in a passive manner. Unlike a RW, the FW rotation is self-propelled without input torque from external power; hence, there is no need for additional input

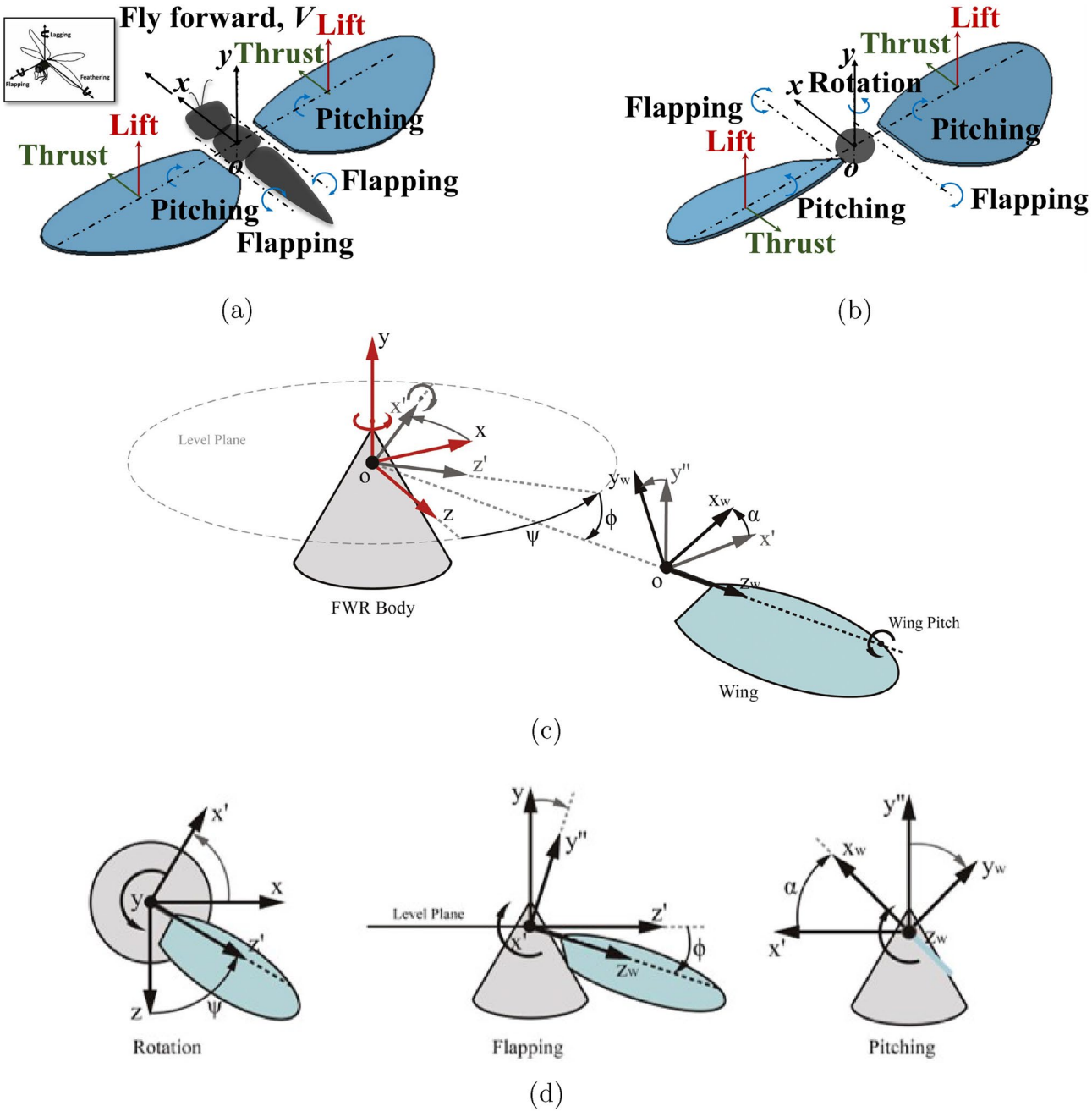

Fig. 2 **a** Sketch of insect forward flight and **b** FWR concept of hovering. **c** Coordinate system and rotation angles definitions for FWR wing; **d** top, back and side view of the Euler angles [27]

power to balance the torque. This leads to the FWR design concept with a simple and power-efficient configuration.

The FWR kinematics of motion presented in a coordinate system used in previous research [27] are shown in Fig. 2c, including the inertial system (x, y, z) attached to the body, the wing-fixed system (x_w, y_w, z_w) attached to the wing root, and the intermediate frame of the Euler rotations (x', y', z') and (x'', y'', z''). The inertial system (x, y, z) and the wing-fixed system (x_w, y_w, z_w) share the same origin o, which is a fixed point at the wing root. The overlapping axes of the intermediate frames y', x'', and z'' are omitted for clarity. The rotating motion is in the x-z horizontal plane. The motion of the FWR is described by sequential rotation about the y-axis (positively anticlockwise), flapping about x, and pitching about z_w axes, with the corresponding Euler angles denoted by ψ (the angle between axes ox and ox'), ϕ (the angle between axes oz' and oz_w) and α (the angle between axes ox' and ox_w) respectively. A planar view with respect to each axis is shown in Fig. 2d.

The FWR kinematics of motion combine flapping, pitching, and rotating angles and amplitudes, which are normally simplified to a sinusoidal motion with a constant rotation speed in most research. The experimental measurement of a mechanical FWR shows that the wing rotation speed is approximately constant under a specified input of flapping and pitching kinematics [31]. Thus, the wing flapping velocity, $\dot{\phi}$, can be represented by a function, $\dot{\phi} = \pi f \Phi \cos(2\pi \hat{t} + \pi/2)$, where f is the flapping frequency, Φ is the flapping amplitude, and $\hat{t}$ is the non-dimensional time ($\hat{t} = ft$, where t is real time). In a previous study by Li and Guo [27], an asymmetric pitching motion inspired by dragonfly wings was employed by modulating the sinusoidal function. The pitching velocity of the wing, $\dot{\alpha}$, is given as, $\dot{\alpha} = 2\ f\left\{(\alpha_u - \alpha_d)(-1)^{[2\hat{t}+0.5]} - \cos(4\pi\hat{t} + [2\hat{t} - 0.5]\pi)\right\}$, where α_u and α_d are the geometric AoA of the wing at mid-upstroke and mid-downstroke respectively. Similarly, Wu et al. [30] manipulated the pitching motion by using a trapezoidal function, with a non-dimensional time $\hat{t}_r$ when reverse starts and a non-dimensional reversal time interval $\Delta\hat{t}_r$ that takes for the AoA changing from α_u to α_d. The corresponding angular velocity, $\dot{\alpha}$, was modelled as: $\dot{\alpha} = 360\ f\left\{1 - \cos[2\pi(\hat{t} - \hat{t}_r)/\Delta\hat{t}_r]\right\}$. The wing kinematics resulting from these two different pitching patterns are depicted in Fig. 3.

2.1.2 Experimental Measurement of Wing Kinematics

Researchers used various measurement methods to collect data on the FWR kinematics of motion and unsteady aerodynamic forces for validation of the aerodynamic numerical model and optimization of the FWR mechanism. A laser sensor/velocimeter with reflective stickers was utilised to

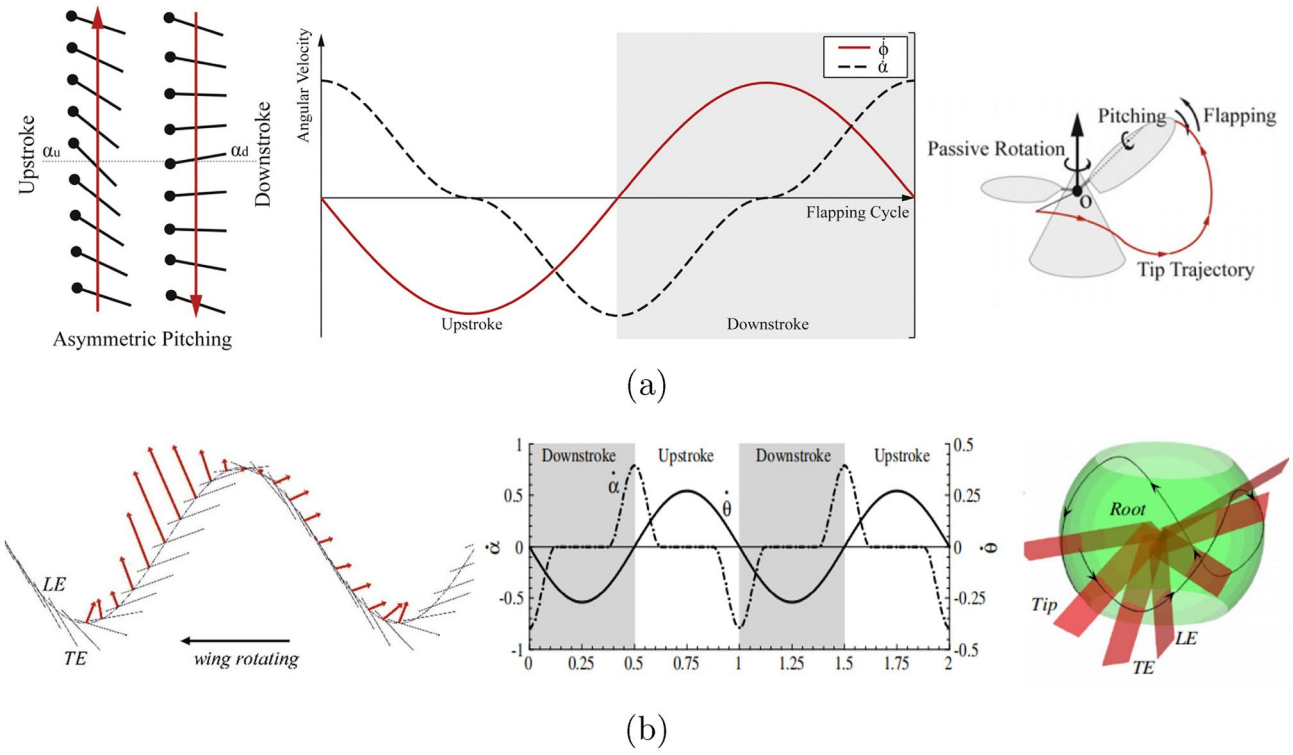

Fig. 3 FWR kinematics adapted from **a** [27] and **b** [30]

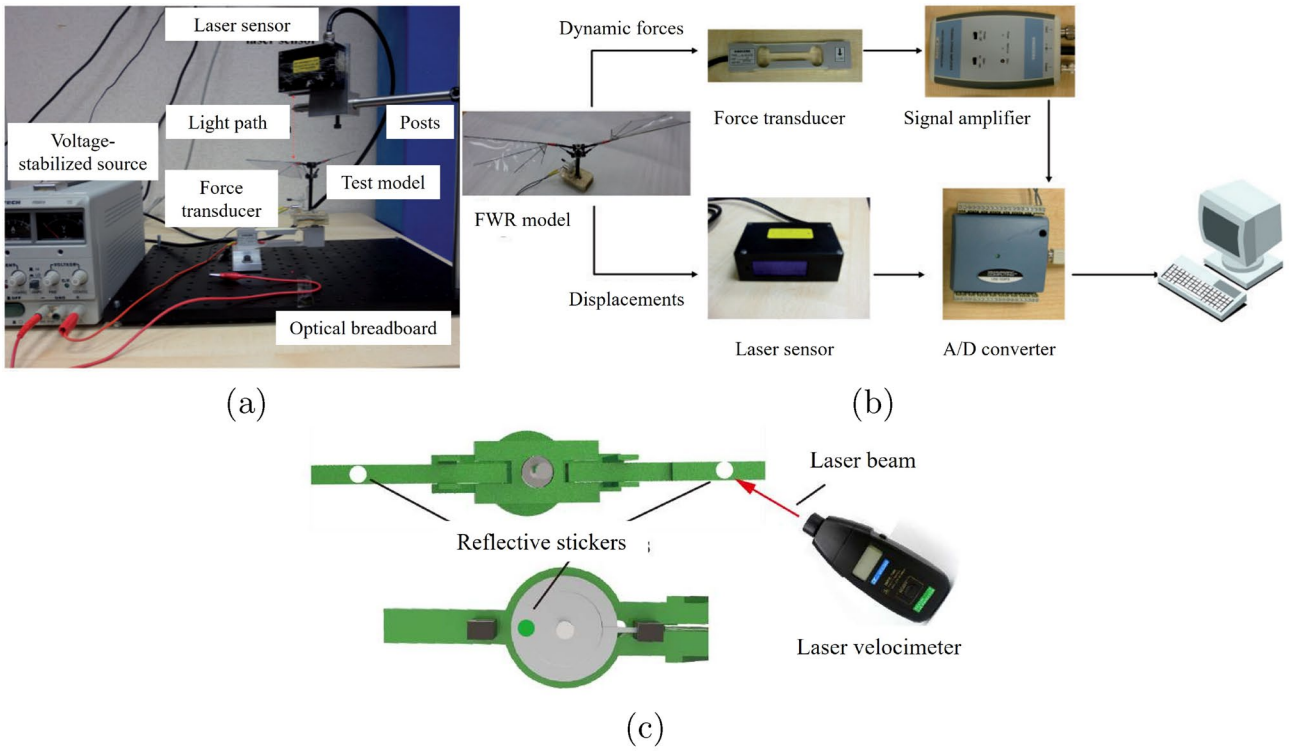

Fig. 4 Experiment setup (**a**) and measurement circuits (**b**) for an FWR model [32]. **c** Rotation speed and flapping frequency measurement by laser velocimeters [33]

measure the flapping frequency and rotation speed of an FWR model [18, 32, 33], as shown in Fig. 4. The model was mounted on a force transducer/load cell, and the data was processed through a signal amplifier and a PC to obtain the vertical force generated by the wings.

Figure 5 illustrates the use of a high-speed camera to capture the instantaneous images of the FWR kinematics of motion, including the flapping, pitching angles and wing deformation throughout multiple consecutive flapping cycles [21]. The experimental outcomes substantiate that the flapping frequency, rotation speed, and time-average lift all increase almost linearly with the input power. The rotation speed varies approximately linearly with the flapping frequency. Due to the aeroelastic coupling between the wing elastic, inertia, and aerodynamic forces, the wing pitching angle varies around the initial geometric AoA (15°).

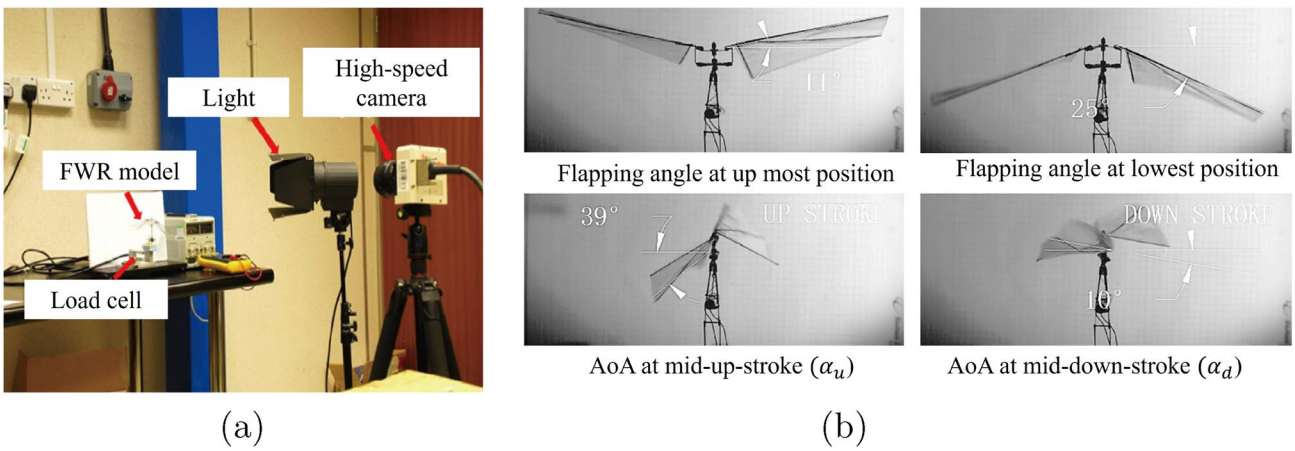

Fig. 5 **a** FWR experiment setup using a high-speed camera; **b** images of instantaneous moments with post-processed flapping angle and AoA [21]

Wu et al. [31, 34] used two synchronized high-speed cameras to capture the motion images and rebuild the position of the FWR, as shown in Fig. 6. Their experiment prevented imaging distortion in the 3-DOF motion. The wing surface was marked, and a program was used to automatically detect and match the marked points between the two cameras, allowing for the determination of the wing position, orientation, and deformation. Their practical FWR model results are showed in Fig. 6b and demonstrate that the flapping angular speed time history follows an approximate trapezoidal function, particularly at the beginning of flapping cycles, but fluctuates during subsequent upstroke/downstroke reversal motion. The aeroelastic effect causes passive pitching of the wings, resulting in significant variation in the pitch angle during a flapping cycle. The pitch angle reaches several peaks at the reversal and the middle of the upstroke/downstroke. Additionally, the rotation speed increases with the flapping frequency and actually varies throughout the flapping cycle.

2.2 FWR Aerodynamic Mechanism

Airborne flapping wings generate unsteady aerodynamic forces, with two main types of kinematics: horizontal and vertical strokes. Many insects, such as hummingbirds, fruit flies, and bumblebees, use a figure-of-eight motion track in a horizontal plane with symmetric wing pitching and identical AoA in VTOL and hovering [35, 36], as shown in Fig. 7a. Their mechanism involves stall delay due to an attached Leading Edge Vortex (LEV), contribution from added mass and rotational circulation, wing-wake interaction, and the clap-and-fling effect [26, 34, 35, 37].

The FWR employs unique kinematics of motion, with flapping up and down strokes and wing rotation, as illustrated in Figs. 2 and 7b. Figure 7b demonstrates that similar to insect flapping wings, the LEV attachment is crucial for FWR to produce high lift. During downstroke, a substantial wing vortex ring comprising the LEV, trailing edge vortex (TEV), and tip vortex is formed, dominating lift production, as shown in Fig. 7c. The main difference between the FWR and insect-like flapping wings is the rotation-induced airflow, which changes the effective AoA and enhances aerodynamic lift and efficiency. Further insights on this aspect are presented in the following section.

2.2.1 High Lift Mechanism of LEV

Researchers often employ the computational fluid dynamics (CFD) method to simulate and depict the structure of the flow field around the wing in detail, as well as the

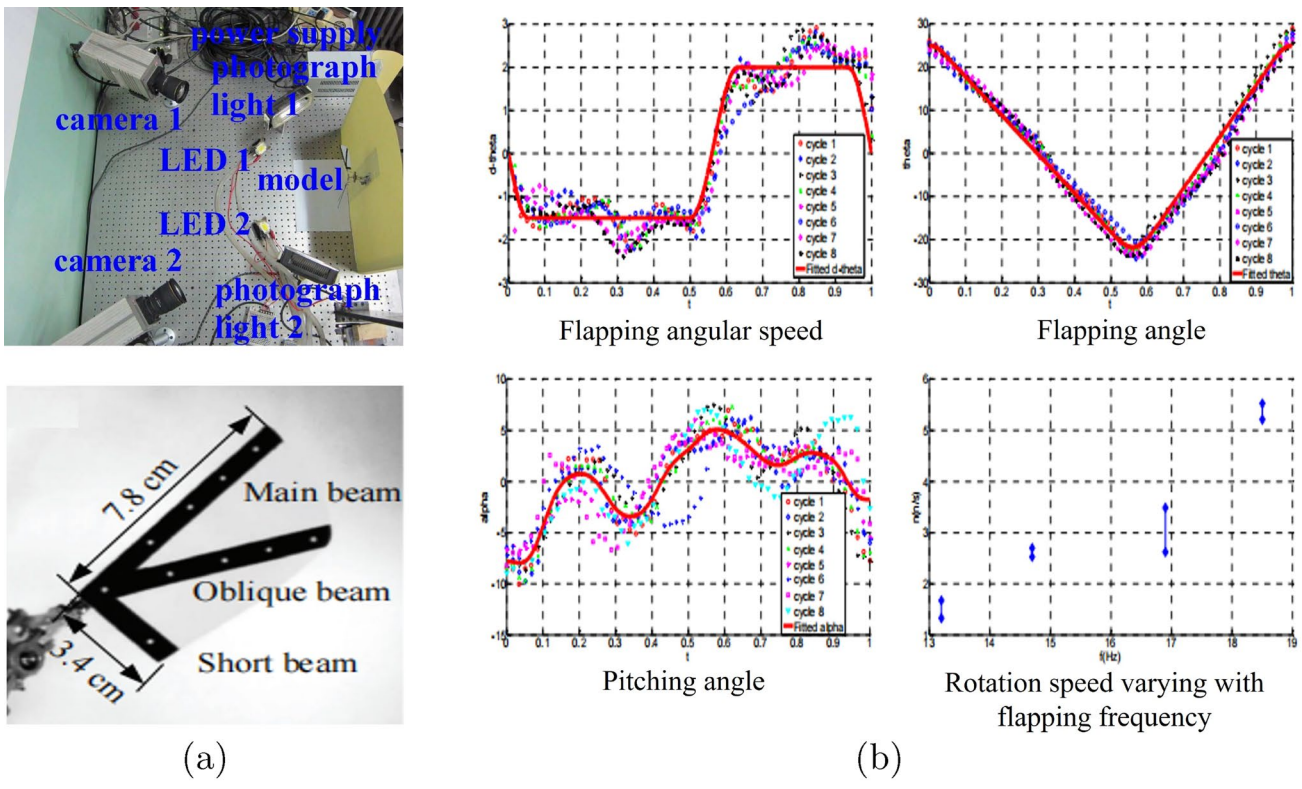

Fig. 6 **a** FWR test platform using two synchronized high-speed cameras and the marked points on the wing; **b** results of wing kinematics of motion [31]

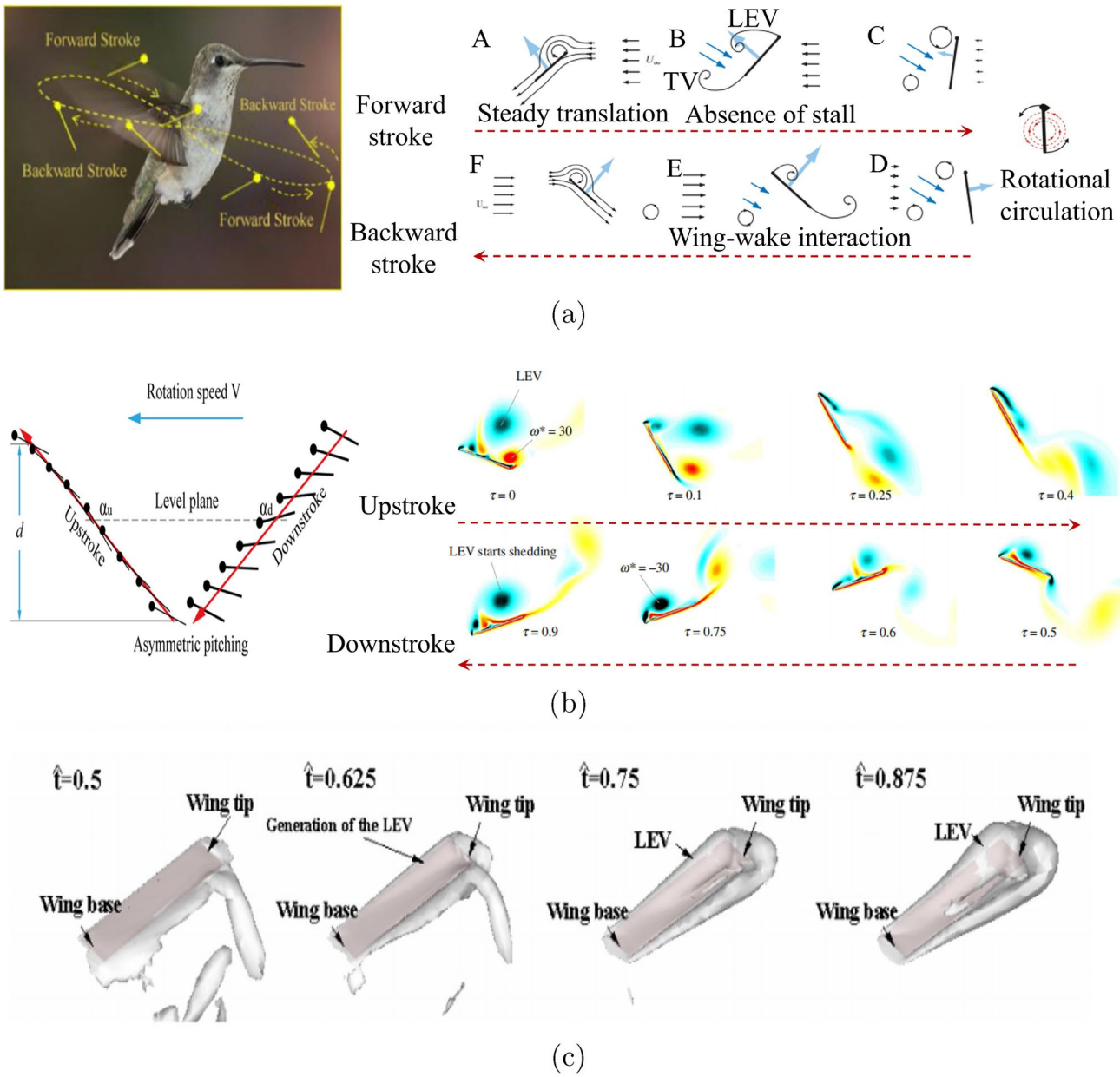

Fig. 7 **a** Hummingbird flight pattern [35] and unsteady aerodynamic mechanisms of insect flight [26]. **b** Contour of flow vorticity for the 2D wing section of the FWR [21, 38]. **c** Variation of the flow field around the 3D FWR wing in downstroke [39]

evolution of vortex and wake, based on incompressible unsteady Navier–Stokes equations. For the FWR, the flow crossing a 2D wing chord exhibits a dynamic history of vortex generation and shedding, as shown in Fig. 7b [38]. As the FWR flaps up and down, the vortex on the leading edge is developed and shed over one cycle after another. The LEV is lost near the end of the downstroke, resulting in a drop in the lift coefficient. The maximum rotation speed is achieved when the wing generates small and symmetric LEVs in the up and downstroke, while the asymmetric larger LEV generated during the downstroke is advantageous for lift production but decreases propulsive efficiency [38].

The positioning of the LEV on either the upper or lower wing surface of the FWR is contingent upon the effective AoA [40]. A strong LEV for high lift production usually forms on the upper surface of the wing and continues to shed until a reverse flow emerges from the trailing edge. The size of the LEV increases as the effective AoA increases and reaches its peak near the middle of the upstroke or downstroke. Furthermore, the effective AoA can keep positive with the LEV generated on the upper wing surface during

the upstroke, owing to higher lift production than the vertical FW [30]. Finally, the pitching motion intensifies the LEV, resulting in more aerodynamic force projection in the direction of lift [41].

2.2.2 Kinematic Effects on FWR Aerodynamics

Several numerical methods, including CFD simulation [27, 30, 38, 40, 42–44] and experimental work [17, 18, 23, 32, 45], have been carried out to study the effect of wing kinematic of motion and mechanical and geometric parameters on the aerodynamics of FWR. Li and Guo [27] adapted a quasi-steady aerodynamic model that considers both translational and rotational effects to predict the time course of FWR aerodynamic forces. The model is based on the assumption that fluid dynamic force depends only on the instantaneous wing motion, including velocity and acceleration. Time-invariant parameters such as translational force coefficients are determined empirically based on the wing geometry and flow conditions, such as the Reynold number (*Re*). The elementary forces along the wingspan are integrated to calculate the total force and torque of a 3D wing based on the 2D FW theory. The lift and rotational moment (torque) coefficients of the FWR are computed as $C_L = L/(0.5\rho U^2 S)$ and $C_M = M/(0.5\rho U^2 S\bar{c})$, where ρ is the air density, U is equal to $2\Phi f R_2$ with the radius of the second area moment R_2, S is the wing area and $\bar{c}$ is the mean chord length. A non-dimensional rotation speed, $\eta = \psi_0/(2\Phi) f$ where ψ_0 is the wing rotation speed in the horizontal plane, is used to indicate the deflection of the effective AoA (α_e).

Li and Guo [27] focused on investigating the effect of the FWR pitching angle on the aerodynamic forces, in an equilibrium state when a constant rotation speed and average rotational moment (torque) coefficient $\bar{C}_M = 0$ conditions are reached. During downstroke, the wing forms a large effective AoA (α_e), contributing to a large lift and rotational moment, while during upstroke, it forms a small positive effective AoA (α_e), generating a small lift and anti-rotating moment, as shown in Fig. 8a. A larger rotation speed (η) in an equilibrium state is associated with a smaller effective (α_e) during up and down stroke (specifically its peak value at $\alpha_u = 9°$ and $\alpha_d = -9°$) but a larger mean lift coefficient ($\bar{C}_L$), as shown in Fig. 8b. Zhao et al. [42] also found that selecting a small pitching amplitude ($\Delta\alpha = \alpha_u - \alpha_d$) of less than 20° and a mean AoA ($\alpha_0 = (\alpha_u + \alpha_d)/2$) of about 40° is beneficial for the FWR to achieve fast rotation speed and produce high lift coefficient, as shown in Fig. 8c.

The effects of rotation speed, flapping frequency, and AoA on the lift production of the FWR were also investigated experimentally. The rotation speed was found to increase approximately linearly with the flapping frequency as more energy was transferred to the system [31], as shown in Fig. 9a. The mean lift produced by the FWR also increased linearly with the flapping frequency and reached a peak value at initial AoA around 15° [32], as shown in Fig. 9b. Beyond this point, the mean lift value gradually decreased but remained high until the AoA exceeded 35°, indicating the occurrence of dynamic stall, in which the wing can travel at a high AoA and generate further lift before stalling [46]. This is due to the stability of the LEV which circulation augments the bound vortex and hence the lift, as characterised by the quasi-steady model of flapping wings [27, 47].

2.3 Aerodynamic Performance of FWR in Hovering and Forward Flight

2.3.1 FWR Hovering Flight Performance Compared with FW and RW

As current MAVs face limitations in payload capability and flight endurance, aerodynamic vertical force and power efficiency are two significant indexes of the performances of various wing configurations. The novel FWR MAV has garnered interest due to its ability to couple flapping and rotation motions to enhance lift production in hovering flight. An experimental study [32] showed that the FWR generates more lift than the superposition lift from purely flapping and purely rotating motions. The lift generated by the FWR is greater than that of a conventional rotary wing at the same rotating speeds in the low *Re* range of 2600–5000, given an appropriate Strouhal number (*St*).

The *St* is a non-dimensional parameter that characterizes the kinematics of wing motion (e.g., stroke frequency, amplitude, and forward flight), which governs the unsteady flow and the shedding of vortices. It is closely related to the propulsive efficiency, which is the ratio of the aerodynamic power output for propulsion to the power input [48, 49]). For an active flapping and passive rotating FWR, high efficiency of lift production is achieved at *St* is between 0.1 and 0.3, which is generally less than the *St* required for high propulsive efficiency (between 0.2 and 0.5) [38].

The aerodynamic power efficiency of FWR is evaluated by calculating the aerodynamic power consumed to counteract the work done by the wing flapping and pitching motions at a certain equilibrium rotation speed. This indicates that the average power consumed by rotating motion becomes zero. The aerodynamic power efficiency is actually denoted by a power factor (P_f) which represents the power work for producing a certain amount of aerodynamic lift force, computed by $\bar{C}_L^{1.5}/\bar{C}_p$ where $\bar{C}_L$ is the average lift coefficient and $\bar{C}_p$ is the average aerodynamic power efficient in a flapping cycle [27]. The aerodynamic power coefficient (C_p) is given as $C_p = \boldsymbol{C_M} \cdot \boldsymbol{\omega}$, based on the moment coefficient ($\boldsymbol{C_M}$) and the angular velocity vectors ($\boldsymbol{\omega}$) in inertia coordinate system

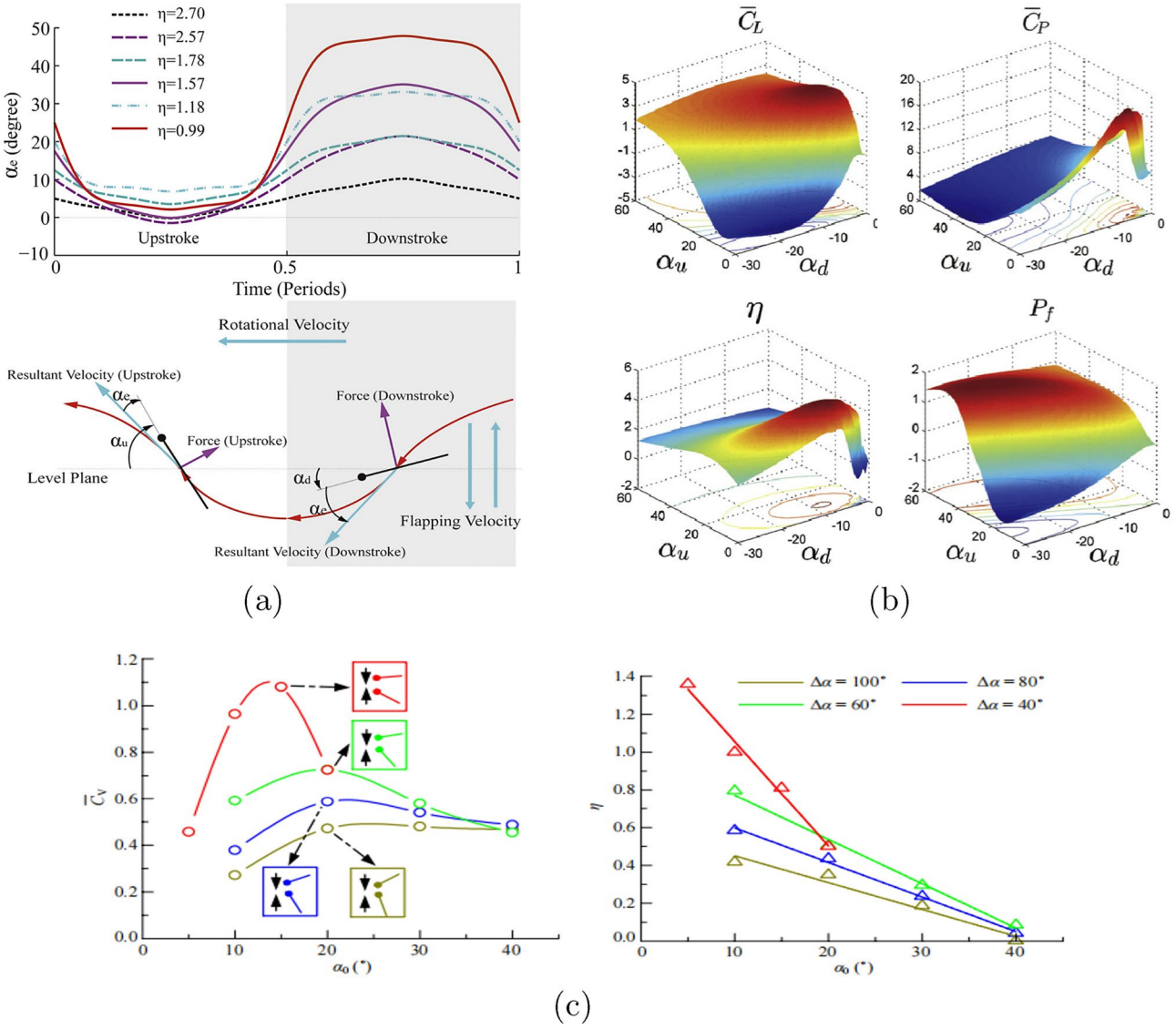

Fig. 8 **a** Variation of the FWR effective AoA (α_e) in one flapping cycle at different rotation speeds (top) and directions of velocity and aerodynamic forces (bottom). **b** 3D surface plots of mean lift coefficient ($\bar{C}_L$), mean power coefficient ($\bar{C}_P$), nondimensional rotation speed (η), and power factor (P_f) in the ranges α_u = 0–60° and α_d = 0 to −30° [27]. **c** Mean lift coefficient (left) and nondimensional rotation speed (right) vary with the mean AoA (α_0) and the pitching amplitude AoA ($\Delta\alpha$) [42]

[30] A higher power factor indicates a more power-efficient system in producing the same average lift coefficient.

Generally, the criterion of maintaining a constant *Re* is used to compare the aerodynamic performance of various MAV configurations in hovering [36, 50, 51]. Li et al. [27] and Wu et al. [30] conducted a comparative analysis of aerodynamic force and efficiency of four types of wings (RW, insect-like vertical flapping-wing (VFW), horizontal flapping-wing (HFW), and FWR) by their average lift coefficient and power factor in the same *Re* (3500 and 2325, respectively). Their results demonstrate that the FWR can produce a significantly greater aerodynamic lift coefficient than other wings, as shown in Fig. 10a, b. Although the RW has the highest power efficiency, its lift coefficient is the smallest, whereas the FWR offers a broader range of combinations of aerodynamic lift and power efficiency with optional kinematics of wing motions. Furthermore, for the FWR, the state of maximum lift efficiency nearly approaches the state of highest aerodynamic power efficiency.

Alternatively, without the constraint of *Re*, Zhou et al. [42] compared the power consumption of RW, FW and FWR for producing a desired lift. They found that FWR and RW can achieve the target lift with less power consumption at an AoA that corresponds to the maximum lift and power coefficients. However, the most power-efficient RW is unable

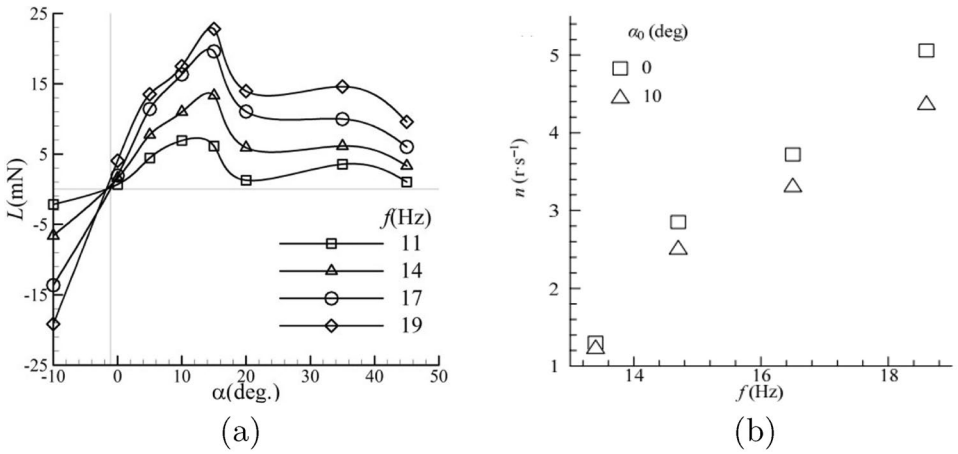

Fig. 9 **a** Rotating speed versus flapping frequency [31]. **b** Variation of lift production with initial AoA in various flapping frequencies [32]

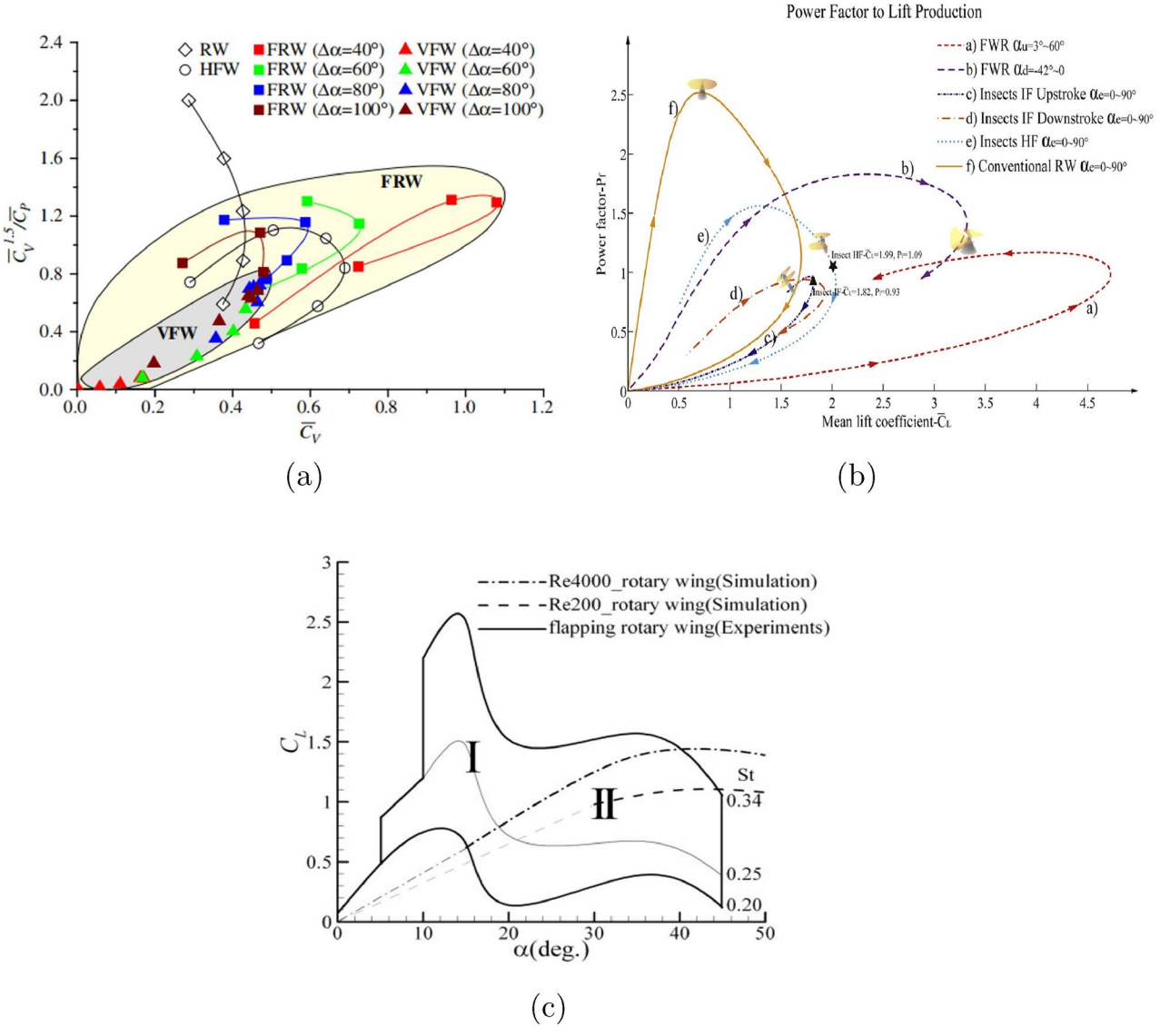

Fig. 10 Performance polar of power factor varies with mean lift coefficient by different types of wings **a** at $Re = 2325$ [30] and **b** at $Re = 3500$ [27]. **c** Comparison of lift coefficient between FWR and RW at different Re [32]

to produce sufficient lift under certain *Re*, as illustrated in Fig. 10c [32].

2.3.2 FWR Forward Flight Performance

Most previous studies on FWR aerodynamics have concentrated on hovering flight, which is an initial flight condition for an aircraft design. To explore practical engineering applications of FWR, Wu et al. [44] conduct a numerical study to investigate the aerodynamic performance of an FWR in forward flight. FWR adopts a forward-tilted rotational plane to fly forward, which is inspired by rotary wings, as shown in Fig. 11a. They evaluated lift, thrust, rotating moment and power consumption, and discussed the differences between hovering and forward flight in terms of the rotational-cycle-average and transient aerodynamics, vortex structure, and pressure distribution on the 3D wing surface.

Similar to hovering flight, FWR in forward flight generates lift and thrust primarily during the downstroke and produces a propulsive rotation moment during the upstroke, with periodic formation and shedding of LEVs as the wing flaps up and down. When rotating at a specified rotation speed, FWR in forward flight experiences a decrease in the rotational-cycle-averaged lift and thrust, but an increase in the rotating moment compared to hovering flight.

In forward flight, FWR exhibits advancing and retreating sides similar to helicopter blades [52], as shown in Fig. 11a. The transient aerodynamics and flow pattern

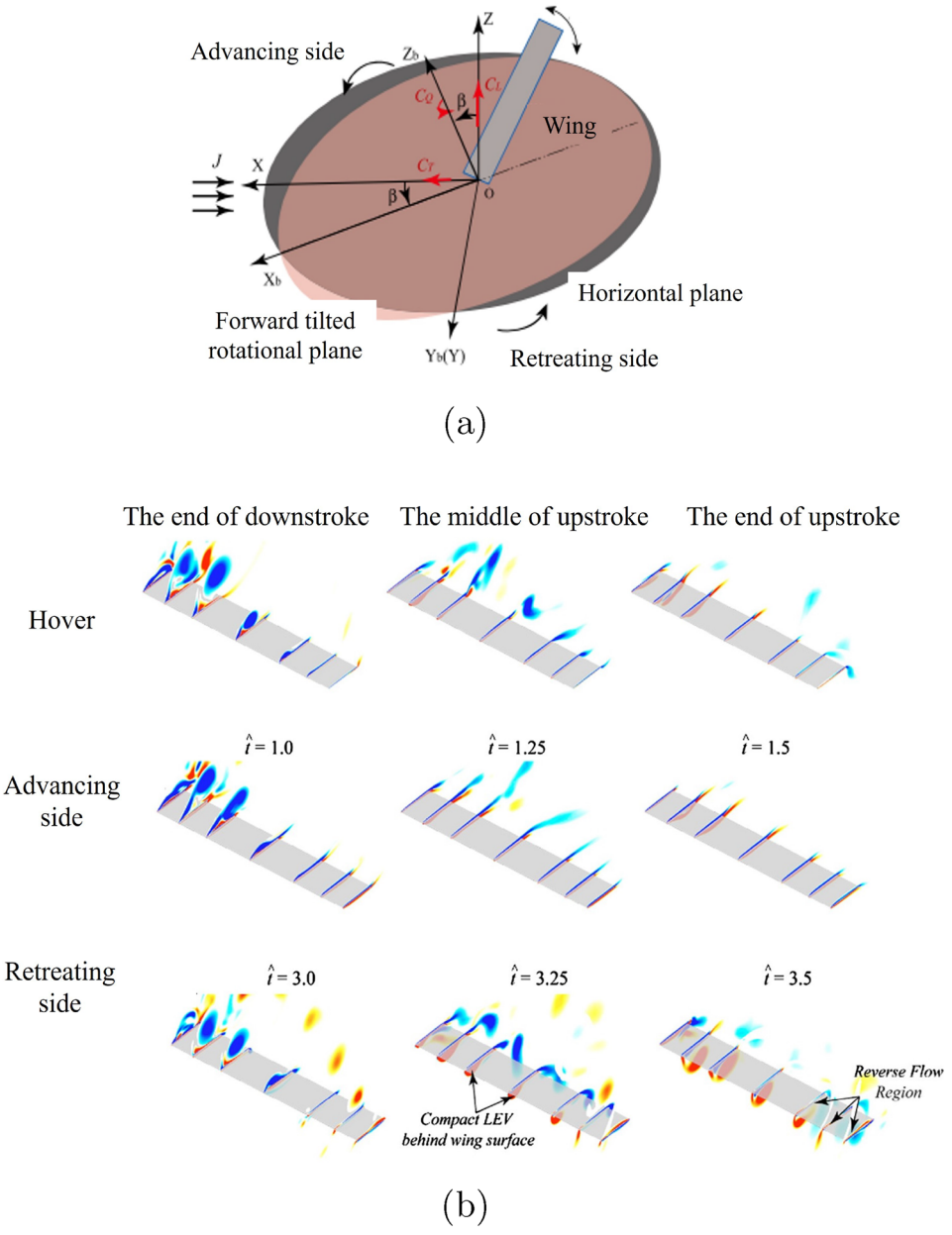

Fig. 11 **a** Coordinate system and kinematics of FWR in forward flight. **b** Vortex structure around the 3D wing during the upstroke of a flapping cycle in hovering flight and forward flight of FWR [44]

on the advancing side of forward flying FWR is approximately the same as those in the hover condition, while on the retreating side, a distinct vortex structure forms near the outer and inner wings at a typical upstroke stance, resulting in a reverse flow region and disappearance of the strong negative pressure area from the wing upper surface. As illustrated in Fig. 11b, this forms an LEV on the wing's lower surface with an area-enlarged pressure region appearing on the upper and lower surfaces, leading to a sharp reduction in lift and thrust and an enhancement of rotating moment. Consequently, the changes in aerodynamics during forward flight compared to hovering flight are primarily due to the significant reverse flow region on the retreating side.

Wu et al. [44] also comprehensively analysed the effects of various wing kinematics such as rotation speed, advance ratio, rotational plane forward-tilted angle and *Re* on the aerodynamic forces, moment, and power consumption of the forward-flying FWR. The funding showed that a moderate advance ratio and a rotational plane forward-tilted angle are crucial for aerodynamic enhancement and power saving.

Typically, FW and RW forward tile the rotating plane by 0°–50° in forward flight [53, 54], with advance ratios ranging from 0.3 to 0.5 [54] and 0.1–0.7 [53, 55], respectively. A forward-tilted rotating plane will project additional lift in the front direction, converting partial lift to thrust. When the FWR operates at a stable passive rotation speed with near-zero rotational moment ($\bar{C}_M$=0), lift, thrust, and power consumption remain nearly unchanged while the advance speed is increased in small advance ratios below 0.6. It can be seen that thrust production of the FWR no longer causes lift loss, and thus, additional control of wing kinematics is no longer required to increase lift to balance the vehicle weight. This differs from purely FW and RW in hovering flight and potentially reduces the difficulty of designing control systems.

FWR can rotate faster at a large rotating plane forward tilted angle, improving lift and thrust production, but if the tilted angle exceeds 30°, thrust no longer increases and there is a loss of lift. The generated lift can remain larger than in hovering when the tilted angle is lower than 30°, allowing for relatively low power consumption. Hence, a rotating plane with a forward tilted angle of around 30° is recommended for FWR to achieve faster forward flight.

The aerodynamic performance of FWR can be fully realized at *Re* greater than 1000, taking advantage of a faster rotation speed to enhance aerodynamic forces. By contrast, the aerodynamic performances of purely FW and RW are not significantly sensitive to advance ratio and rotational plane forward-tilted angle, and both effects are generally ignored at *Re* less than 1000. Despite this investigation of aerodynamic performance in forward flight, the flight control strategy and relevant dynamic analysis for FWR in forward flight have been underdeveloped and remain a gap.

2.4 Lift Enhancement Methods

2.4.1 FWR Wing Geometric Optimisation

Research on FWR has mainly focused on optimizing wing kinematics to improve lift production and aerodynamic efficiency. However, most theoretical and experimental analyses have relied on simple rectangular-shaped wings [40–42, 56], or on assumptions and experiences derived from insect-like flapping wings [21, 27, 32]. There is a need for a detailed design and analysis of wing surfaces to optimize aerodynamic characteristics and maximize FWR aerodynamic advantages. In this regard, the wing geometric parameters, including the aerofoil camber, shape of the plane surface, aspect ratio, and twist angle, are crucial design metrics as they significantly affect the aerodynamic performance of FWR.

Firstly, numerous studies of flapping wings show the importance of camber deformation in producing aerodynamic forces. Dragonflies, for example, exhibit considerable camber deformation during free flight, which plays a crucial role in generating vertical force and thrust [57]. Similarly, a study on bumblebee flight has shown that a deformation of 6% camber and 20° twist can enhance lift by 10–20% and reduce the required aerodynamic power for bumblebee hovering flight by 16% [58]. By adopting appropriate camber, flapping wings can gain aeroelastic effects from asymmetric flexibility of camber variation and twist deformation to improve aerodynamic performance [41]. Particularly, an additional positive camber variation in upstroke (9% camber at mid-upstroke) can reduce the negative lift during the upstroke by 22%.

Studies on the effect of camber on FWR aerodynamics have found that adopting appropriate camber can generate more lift than a planar wing [43, 59]. Through the studies on the effect of camber on the FWR wing aerodynamics, adopting appropriate camber can generate more lift than the planar wing [43, 59]. The mean lift coefficient increases as the maximum camber increases within 25% of the chord length, with the maximum lift increasing by 40%. This is because the maximum camber significantly impacts the size and strength of the LEV, which delays vortex shedding and enhances lift production. The increasing camber also affects the mean rotating moment coefficient, resulting in a significant increment.

In addition to camber design, the aerodynamic performance and flow pattern of FWR are influenced by different wing area moments [43, 60]. The radius of the second area moment, which indicates the wing's tapered ratio between

the tip and root chords, has a significant impact on the mean lift coefficient. The mean lift coefficient increases as the increasing tapered ratio enhances the LEV, whereas a large-tapered ratio results in a small mean rotating moment even as the Re increases. Therefore, Wang et al. [43] suggested that a moderately tapered ratio forming a nearly rectangular wing is optimal for FWR.

Also, a moderate aspect ratio of 5 is recommended for FWR wing design at a low *Re* [43]. A small aspect ratio produces high lift but low rotation speed. In contrast, a large-aspect ratio increases rotation speed but also considerably increases the effective AoA, leading to a decrease in lift.

Increasing the twist angle of the wing plane, which is the angle between the root and top chords of the wing, enhances the mean lift coefficient of FWR by strengthening and weakening the LEV attached above and below the wing surface during downstroke and upstroke, respectively. To balance both lift and rotating moment production, a slight positive twist angle is recommended for the FWR wing [43]. This is in agreement with the design of selecting 10°–15° initial AoA for FWR to improve lift at a fast rotating speed [32]. Overall, the above methods of optimizing wing geometric parameters to increase lift rely primarily on the mechanism of maintaining high lift production during the downstroke and minimizing negative lift during the upstroke.

2.4.2 Wing Surface Hore–Hole Design for FWR

An alternative method for improving lift generation in flapping wings involves creating perforations in the wing surface [61]. Chen et al. [45] experimentally examined the feasibility of this solution for FWR in hovering, namely passive flow control strategy. They implemented a bore-hole design on FWR by perforating the membrane wing and covering the hole with a film that opened during the upstroke to unload negative aerodynamic force and closed during the downstroke to maintain lift generation, as shown in Fig. 12a. The lift enhancement achieved by the perforated wing was dependent on initial AoA, position and size of boring holes, and covering film material, resulting in a 35% increase in average lift.

Chen et al. [62] further investigated the effect of the bore-hole design on the aerodynamics of FWR during forward flight. They found that lift enhancement of the FWR with bore-hole design could be maintained within certain limits of advance ratios and tilt angles of disk plane. The lift enhancement during upwind flapping cycles is considerably more significant than during tailwind flapping cycles. Like hovering flight, they observed a significant reduction in negative lift during the upstroke of upwind flapping cycles, attributed to the release of pressure difference and the formation of a low-pressure region on the wing's upper surface, as shown in Fig. 12b. Increasing the effective AoA lifted the secondary LEV, which reduced the low-pressure region. However, the bore-hole design reduced the rotational torque during upwind flapping cycles. They suggest that a meticulous material and structure design for the hinge can achieve appropriate passive deformation to prompt the reduction of negative lift during upstroke.

2.4.3 Twistable Flexible Wing for FWR

Flexible wings, typically made of membrane material, are commonly used in physical FW and FWR models. As the wing flaps up and down, the film and spar of the wing undergo complex aeroelastic effects, resulting in distortion. The advantages and disadvantages of a flexible wing depend on the coupling of its strength, stiffness, and deformation pattern with unsteady aerodynamics. Therefore, the effective utilization of flexible wing deformations to improve lift and efficiency and to achieve a more authentic bionic structure

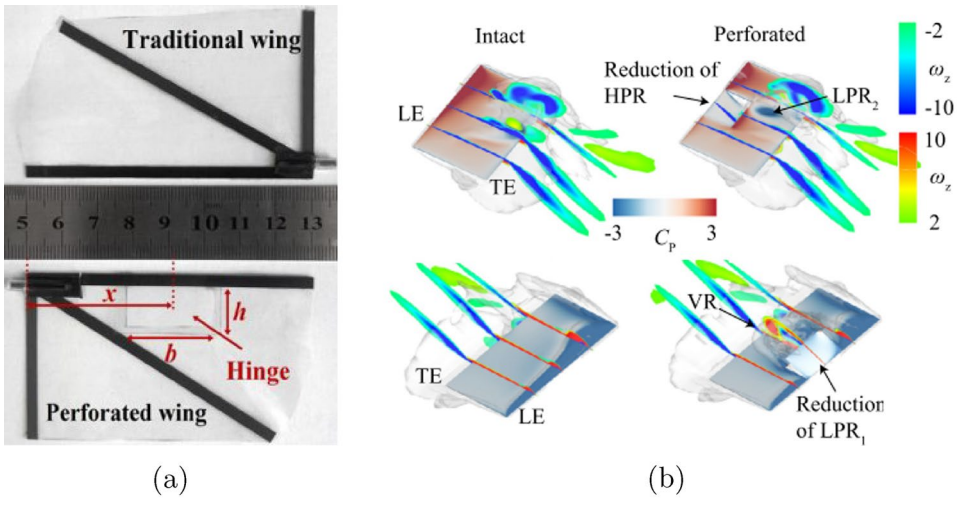

Fig. 12 **a** A bore-hole design for FWR to increase lift [45]. **b** Flow structures of intact and perforated wings in an upwind flapping cycle at the end of upstroke [62]

represents a crucial structural principle and design guideline for advancing FW and FWR design.

In fact, in most previous studies on FWR, the wings were modelled as rigid, and fewer studies have investigated the contribution of wing flexibility. Current studies [63, 64] developed a computationally efficient fluid–structure interaction model to investigate the effect of passive twisting of the wing on the aerodynamic performance of FWR by solving the elastic deformation of a twistable wing, as shown in Fig. 13. Using the verified quasi-steady aerodynamic model, they identified the significant role that wing-root stiffness plays in aerodynamic performance. Their findings showed that higher wing-root stiffness values allowed the twistable wing to generate comparable lift to a rigid wing at a higher efficiency. Therefore, the stiffness design of a twistable FWR wing should be associated with its operating wing kinematics to achieve the desired aerodynamic performance. However, the performance of twistable FWRs is more sensitive to changes in flapping frequency, as an increase in frequency can significantly increase power consumption and decrease efficiency. Additionally, the recent experimental tests [65] on flexible FWR wings quantitatively assessed the impact of chordwise and tip stiffness on aerodynamic performance. The results emphasize that by optimizing stiffness distribution, the FWR's aerodynamic lift and efficiency can be significantly improved.

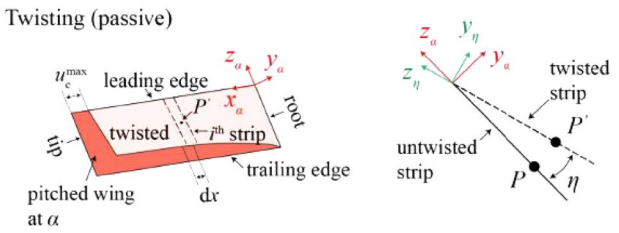

Fig. 13 Schematic diagram of wing spanwise twisting [63]

2.4.4 Passive Pitching Variation of FWR

Although the pitching angle variation is a kinematic parameter of the wing, the dynamic passive pitching manner of the wing is primarily due to elastic deformation. Numerous studies have been conducted to investigate the effects of passive pitching or twist angle variation on the lift and efficiency of flapping wings and rotary wings, as well as to utilize morphing wings [66–68]. The implementation of twisting flapping wings has been found to enhance lift by over 25% and generate a higher thrust-to-drag ratio [66]. Wu et al. [31] analysed the flow structure around the wing of an FWR by the CFD method, and demonstrated that passive wing pitching is beneficial for FWR to augment lift. Chen et al. [23] built a novel sleeve-pin unit mounted on the end of a U-shaped flapping mechanism of the FWR (Fig. 14), allowing the wing to twist freely around the wing spar axis, and conducted measurement experiments.

The passive pitching angle variation (PPAV) of the FWR resulted from aerodynamic pressure and inertia force during upstroke and downstroke and was found to significantly increase mean lift and power efficiency by reducing the negative aerodynamic lift generated during upstroke in comparison to a constant pitching angle. Notably, the mean lift and aerodynamic efficiency were more than 100% higher than the baseline FWR when the input voltage was below 6 V. Additionally, utilizing a lighter wing with a higher flapping frequency produced more lift with reduced inertia force and power demand than a heavier wing under the same input power.

2.4.5 Asymmetrical Flapping Motion of FWR

All previous studies on FWR have utilized symmetrical flapping motions where the maximum and minimum stroke angles are identical. In contrast, the FWR model developed with PPAV [23] has an asymmetrical flapping motion, with a maximum stroke angle of −20° above the horizontal plane

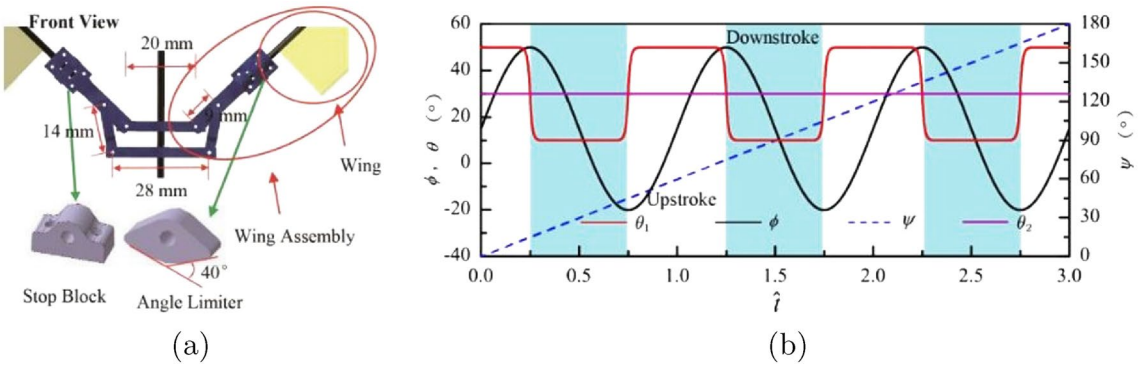

Fig. 14 **a** Sleeve-pin unit for PPAV and U-shaped mechanism. **b** Wing kinematics of motion [23]

and a minimum stroke angle of 50° below it, as shown in Fig. 14. This asymmetry in flapping motion is another crucial factor that contributes to the high lift and successful take-off flight of the FWR model.

The authors' experimental measurements of an updated FWR model have validated the kinematic optimization of asymmetrical stroke amplitudes, as demonstrated in Fig. 15a. Case 1 employed a symmetrical flapping motion with a stroke angle range of −40° to 40° and a pitching angle variation of 0°–35°, whereas Case 2 employed asymmetrical flapping motion with a stroke angle range of −30° to 40° and a pitching angle variation of 7° to 42°. As depicted in Fig. 15b, optimized Case 2 produced twice the total force, which includes both lift and inertial forces, as compared to Case 1. The tested FWR model with optimized motions was capable of producing sufficient lift and achieving a series of free flights, as discussed in later Sect. 3.2.

2.4.6 Elastic Mechanism for FWR

The small size and light weight of MAVs present a significant challenge to their flight capability and endurance due to the limited output and energy capacity of portable power sources. To address this challenge, researchers have taken inspiration from insects, which minimize flight energy using flight muscles, flight thorax, and wing hinges. Recently, elastic energy storage has been implemented FW MAVs, and a compliant mechanism driving the flapping mechanism at the resonant frequency has been shown to be an effective power-saving technique [69–72].

The author implemented the concept of elastic energy storage by integrating springs into the driving mechanism of a mechanical FWR, as shown in Fig. 14a. The experimental results showed that the FWR mechanism achieved a significant reduction in input power from the motor by utilizing the springs to accelerate or decelerate the wing motions, as compared to the baseline model without springs at the same flapping frequency, as shown in Fig. 16b, c. The study also demonstrated the resonant characteristics of the elastic FWR mechanism, with a 50% reduction in power consumption compared to the baseline model. By optimizing the stiffness, the study achieved a 16% increase in power efficiency (the ratio of lift to input power) compared to the baseline model while obtaining the same aerodynamic lift force.

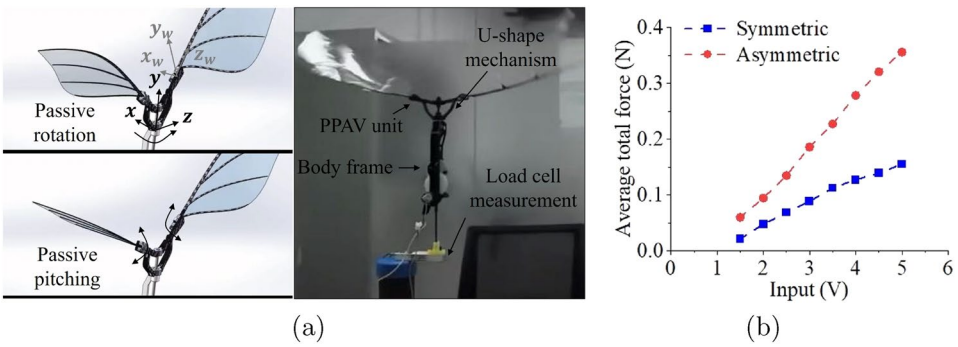

Fig. 15 **a** Tested FWR model. **b** Average total force of the FWR model over a flapping cycle in a range of input voltage

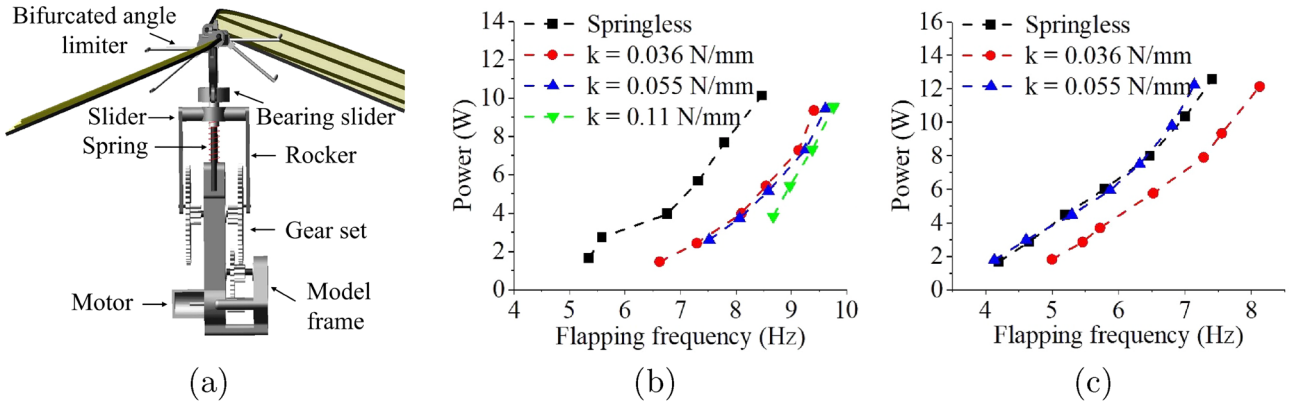

Fig. 16 **a** Elastic mechanism for FWR. Variation of input power with flapping frequency of the FWR model with various spring stiffness: **b** without skin cases and **c** with skin cases

3 Flyable FWR MAVs Development

3.1 Mechanical FWR and Flight Test

Typically, a physical FWR model comprises an FW mechanism and a driving mechanism. A DC motor rotation is converted to linear reciprocating motion through a pushrod and transformed into wing flapping motion via a U-shaped mechanism that permits passive wing rotation around a central shaft. The flapping rotary mechanism is a typical four-bar linkage mechanism, i.e., a U-shaped frame. High-speed, low-voltage propulsive actuators such as micro-coreless and brushless motors are commonly used in FWR models. Due to the heavy load of FWR mechanisms, a gearbox is often employed to reduce motor speed and increase output torque for driving the transmission of a crank-linkage mechanism.

Guo et al. [21] designed and manufactured the first flyable FWR model in 2014, which weighed only 2.6 g and was powered by a micromotor via fine wires. Despite its small size, it was able to generate sufficient lift force for a successful vertical take-off and remain airborne for a short period, as shown in Fig. 17a. During flight, the FWR had a flapping frequency of 21 Hz, a rotation speed of 7.2 r/s, and a power consumption of 2.6 W. This achievement was a significant milestone in the research and development of FWR MAVs, demonstrating the feasibility of the unique features of the FWR concept in terms of flight dynamics and stability.

Subsequently, Yi et al. [73] integrated a motor with a lithium micro battery on the FWR platform, with a total weight of 21.51 g, achieving vertical take-off and upright flight with an onboard power supply for the first time, as shown in Fig. 17b. However, due to the lack of altitude and attitude control components and a remote or automatic system, the model quickly became unstable and fell.

Dong et al. [22] advanced a linkage-driven three-wing FWR of 32 g with an onboard power and flight control system, as shown in Fig. 17c. The controlled FWR was equipped with an attitude control mechanism, including stabilizers and rudders driven by servos located below the body base. With the help of a lightweight coin-sized flight control board, the FWR successfully performed free-controlled hovering and forward flight, marking a significant milestone in the engineering development of FWR MAVs. However, this FWR primarily relied on adding an extra wing to increase lift production to perform a free flight and did not fully highlight the aerodynamic and efficiency advantages of the FWR concept. They extended their research on a smaller-scale FWR equipped with two wings directly driven by two bi-directional rotating brushless motors [74]. This design operates at twice the flapping frequency and has successfully achieved controlled flight, as shown in Fig. 17e.

The above physical FWR models have a fixed AoA and cannot change their pitching angle by twisting their wings along the leading edge. Using the lift enhancement unit of passive pitching, the two-wing FWR contrasted by Chen et al. [23] achieved a 2-s vertical takeoff and hovering flight, as shown in Fig. 17d. Despite being powered by 9 V input voltage through wires and weighing 22.7 g (with 4 g of wires), this FWR model demonstrated significant potential for developing an enlarged magnitude of FWR MAVs due to its high lift coefficient.

Our recent advancements in FWR MAVs are exemplified by the integration of PPAV's lift enhancement and

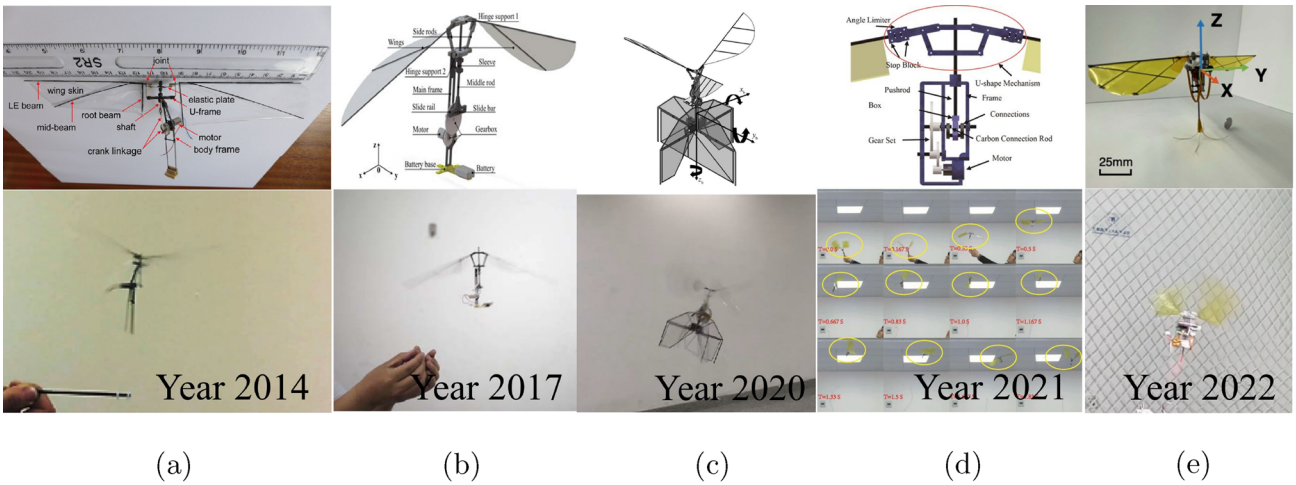

Fig. 17 **a** First and lightest tethered flyable FWR [21]. **b** First untethered flyable FWR [73]. **c** A linkage-driven three-wing flyable FWR [22]. **d** A flyable FWR with PPAV [23]. **e** A motor direct-drive two-wing flyable FWR [74]

Fig. 18 Free flights under the remote control of **a** a 25 g single-motor FWR and **b** a 51 g dual-motor FWR with the same pair of wings

asymmetric flapping, as introduced in Fig. 15a. This FWR mechanism equipped with an uncontrolled tail, a single motor, battery, and remote-control device, weighs 25 g and has achieved a remote-controlled flight duration of 7 s (Fig. 18a). With an increase in vehicle weight to 60 gs, its dual-motor model was built, achieving airborne stability for 2.2 s through dual-motor transmission. Enhancements in weight reduction and a remote control system further extended the flight endurance of this dual-motor MAV to 35 s (Fig. 18b). Comprehensive exploration of these models will be the focus of future studies. With our present models, a summary of flyable FWR MAV data can be found in Table 1.

3.2 Free Flight Capability and Endurance Compared with FW MAVs

FW MAVs are typically less than 1 m in wingspan and weigh less than 2 kg [5], and their flight capability and endurance vary. Recent advances in the research and development of FW MAVs have been adequately summarized and discussed in earlier reviews [66–69, 75]; yet, only a small fraction of the fabricated physical models in the literature can conduct the flight. Phan et al. [68] surveyed 28 insect-like tailless motor-driven FW MAVs developed between 2005 and 2018, of which 70% were flyable. These flyable vehicles were categorized based on onboard or off-board power unit and level of flight as guided take-off, tethered flight, passively stable flight, wired controlled flight, and free-controlled flight. Currently, 60% of flyable insect-like FW MAVs can perform controlled flight using onboard electronics and power systems, representing the greatest accomplishment in the research of FW MAVs.

The FWR is a composite MAV wing layout that combines features of flapping and rotary wings. Despite its novelty, it has undergone rapid development in recent years, keeping pace with advances in FW MAVs. It took 5 years for the research team from the FWR concept to achieve the first flight of a 2.6 g prototype. It took another 5 years to increase the maximum take-off weight to 60 g.

In comparing flyable FW MAVs and FWR, bird-tailed FW MAVs are disregarded due to their incapacity for hovering flight. As depicted in Fig. 19, recent advances in insect-inspired tailless FW MAVs capable of free-controlled flight,

Table 1 Data for flyable FWR models

FWR	Wing number	Flapping mechanism	Mass (g)	Power supply	Control	Flight endurance (s)
Guo's model [21]	2	Crank-slider and linkage	2.6	Coreless motor, tethered	Non	–
Yi's model [73]	2	Crank-slider and linkage	21.51	Coreless motor, onboard battery	Non	–
Dong's model [22]	3	Crank-slider and linkage	32	Brushless motor, onboard battery	Free-controlled	42.5
Dong's direct-drive model [74]	2	Dual-motor direct drive	12.5	Brushless motors, onboard battery	Free-controlled	–
Chen's model [23]	2	Crank-slider, linkage and PPAV	22.7	Coreless motor, tethered	Non	2
Single-motor tailed FWR	2	Crank-slider, linkage and PPAV	25	Coreless motor, onboard battery	Free-controlled	7
Dual-motor FWR	2	Crank-slider, linkage and PPAV	60	Coreless motors, onboard battery	Free-controlled	2.2
Dual-motor tailed FWR	2	Crank-slider, linkage and PPAV	51	Coreless motors, onboard battery	free-controlled	35

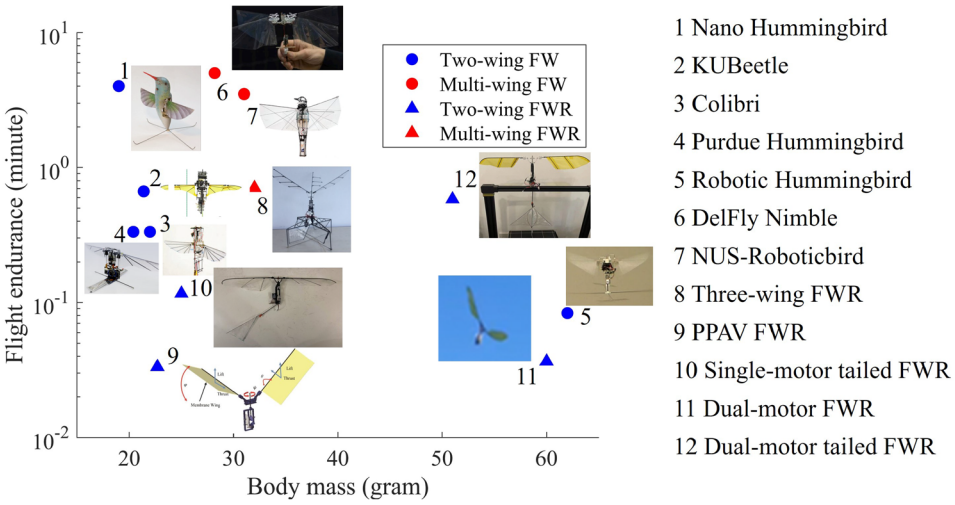

Fig. 19 Flight endurance of free-controlled hovering, insect-inspired tailless FW MAVs (1 [11], 2 [37], 3 [78], 4 [79], 5 [77], 6 [76], and 7 [80]) as well as free VTOL FWR MAVs with or without control system (8 (untethered-controlled) [22], 9 (tethered without flight control) [23], 10 (untethered-controlled), 11 (onboard power supply but without flight control), and 12 (untethered-controlled))

sourced from reputable publications, reveal a two-wing configuration for vehicles weighing under 25 g, while those over 25 g require additional wings for adequate lift. The Nano Hummingbird weighing 19 g, with two wings, boasts the longest flight endurance of four minutes for a small magnitude (< 25 g) FW MAV [11]. In contrast, the most sophisticated and representative insect-like tailless FW MAV at a relatively large magnitude (> 25 g), the Delfly Number, weighs 28.2 g and has four wings enabling a flight time of five minutes and quick turns [76]. Available FWR MAVs have been capable of free-controlled vertical takeoff and hovering in the weight range between 25 and 60 g, relying on just two wings to create adequate lift force. Despite being the heaviest insect-inspired tailless FW MAV at 62 g, the two-wing robotic hummingbird can only fly for five seconds due to a heavy load [77], while the FWR MAV at the same magnitude of take-off weight can have a longer flight. Thus, the superior lift production capabilities of FWR MAVs render them more capable of achieving high flight endurance and performance compared to conventional FW MAVs.

When comparing the body weight and size of two-wing FW MAVs and two-wing FWR MAVs, it is evident that FW MAVs have a larger wingspan than the equivalent weight category FW MAVs, as depicted in Fig. 20. Heavier vehicles require longer wingspans. Furthermore, Purdue Hummingbird (Fig. 20(4)), which has comparable weight and wingspan to Nano hummingbird (Fig. 20(1)) and KUBeetle (Fig. 20(2)), utilizes two motors but has a shorter flight endurance of only 20 s, compared to the 4 min and 40 s of Nano hummingbird and KUBeetle, respectively. This indicates that additional motors might not necessarily enhance the aerodynamic performance of FW MAVs.

In contrast, FWR MAVs can perform flight with the same pair of wings, irrespective of whether they are using the lighter single-motor configuration (Fig. 20(11)) or the

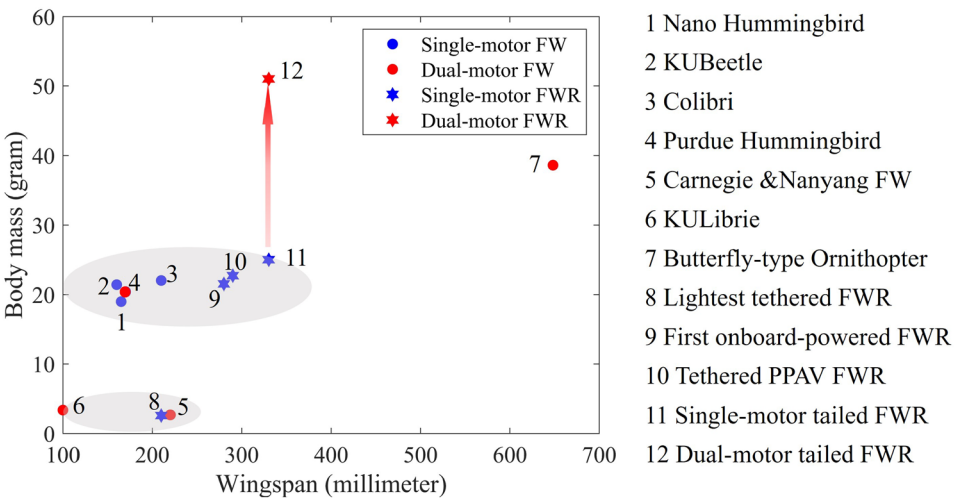

Fig. 20 Wingspan and body mass of two-wing insect-inspired tailless FW MAVs capable of takeoff and hovering (1 [11], 2 [37, 78], 4 [79], 5 [81], 6 [82], and 7 [83]) and free-flight two-wing FWR MAVs(8 [21], 9 [73], 10 [23], 11, and 12)

heavier dual-motor configuration (Fig. 20(12)). Applying an additional motor not only dramatically enhances the aerodynamic lift force, but also extends the flight endurance and doubles the payload capability of Nano hummingbird and DelFly Nimble. Clearly, FWR has a substantial advantage in aerodynamic forces and efficiency. Although the flight endurance and control capability of FWR MAVs are not yet comparable to those of Nano hummingbird and DelFly Nimble, the FWR configuration is highly promising for expanding the payload capacity of MAVs, offering a wide range of applications in the near future.

4 Ongoing Research and Future Development

While recent advances in bio-inspired FW MAVs are noteworthy, practical application in complex environments remains challenging, as they cannot fully emulate genuine flying insects. Literature [37, 84] proposes eight competencies essential for FW MAVs to fulfil real-world application demands: obstacle avoidance or stable flight recovery after wing collisions, extended flight endurance, various locomotion modes (e.g., jumping, running, walking, crawling, swimming, and perching), autonomous flight, low-noise capabilities, multi-vehicle coordination, wind disturbance rejection, and low-density environment navigation. Current FW MAVs can achieve takeoff, hovering, and maneuvering, but lack multifunctionality. Obstacles to agile flight persist in two domains: improving aerodynamics and efficiency and overcoming limitations in micro-scale electronics and power supply technology.

4.1 Research on Bionic Elastic Structure for Improving FWR Performance

Limited flight endurance is a prevalent issue for bio-inspired MAVs due to aerodynamic lift and power efficiency constraints. As discussed in Sect. 2.4.1–2.4.5, optimizing wing kinematics and geometric parameters can enhance the aerodynamic performance of FWR MAVs. Considering wing inertia and the FWR system's power efficiency, employing an elastic actuator to reduce power consumption, as introduced in Sect. 2.4.6, is crucial for energy-effective flight. This allows longer flight durations despite onboard energy limitations, due to efficient propulsion and power usage.

Future research should delve into biological wing structures and flexibility to improve lift production and efficiency, applicable to both FW and FWR vehicles. Previous research on twistable wings for FWR has primarily focused on analyzing twisting deformation and wing-root stiffness, with earlier FWR studies employing rectangular wing planes. The authors are currently investigating the impact of bio-inspired wing shapes and flexibility on FWR aerodynamic performance, seeking to offer a comprehensive understanding of aerodynamic mechanisms stemming from elastic deformation and guidelines for designing biological flexible wings that yield enhanced aerodynamic benefits for FWR MAVs.

4.2 Research on Flight Control and Stability System of FWR MAVs

A major obstacle for existing FWR MAVs is the absence of a well-designed attitude control mechanism specifically tailored to their unique combination of flapping and rotary wings, along with feedback controllers for attitude and altitude regulation. Considering the inherent dynamic instability of flappers, continuous stability control and agile maneuvering control are essential and challenging aspects of designing an onboard control system for innovative FWR MAVs.

FWR MAVs necessitate an active control system capable of adjusting wing kinematics during flight, resulting in the generation of control torque for attitude changes. In the three-wing FWR MAV built by Dong et al. [22], the attitude control mechanism incorporates stabilizers and rudders beneath the FWR driving mechanism, functioning as a tail. The attitude control mechanism incorporates stabilizers and rudders beneath the FWR driving mechanism, functioning as a tail. In their two-wing FWR MAV [74], bi-directional rotation motors drive wing flapping motion, which can be regulated by altering the motors' input voltage. The kinematic disparity between the two wings generates control torques for attitude adjustments and vehicle stabilization. These control strategies resemble those employed by most insect-like FW MAVs, which tilt the stroke plane to transition between hovering and forward flight and execute maneuvers.

Building upon the established FWR platform devised by the authors (Fig. 18a), the project advances by incorporating a control method for transitioning from hovering to cruise flight mode. This pioneering flight scheme employs FWR mode for takeoff and hovering, and FW mode for forward flight, maximizing aerodynamic efficiency of both configurations within their respective flight modes. With nearly horizontal tail stabilizers and control surfaces, this FWR MAV more closely resembles a bird-like FW MAV while retaining efficient takeoff and hovering capabilities. The control system enhances adaptability in various environmental conditions and operational scenarios, thus expanding the potential applications of FWR MAVs. This innovative design serves as a foundation for future research and development, promoting further advances in the field of bio-inspired aerial robotics.

5 Conclusion

This review provides a comprehensive analysis of the FWR, a pioneering MAV design combining bio-inspired flapping and rotational motions, highlighting its aerodynamic efficiency. Distinct from traditional flapping wings, FWR capitalizes on swift passive rotation induced by active flapping, optimizing lift with reduced aerodynamic power. Our exploration underscores FWR's unique aerodynamic mechanisms, emphasizing variations in wing kinematics and performance in both hovering and forward flight in contrast to insect flight patterns. Enlightened by these insights, we delve into advanced lift enhancement technologies that underpin the modern, efficient FWR models. In comparison to established flapping wing models, FWR showcases potential benefits in power efficiency and increased payload capacity. However, challenges persist, rooted in weight and size constraints, intricate flight dynamics, and a paucity of defined control strategies. This review culminates in a detailed discussion on bio-inspired improvements in FWR MAVs, emphasizing flexible wing design and controls that mimic natural entities. This exploration is pivotal for harnessing FWR's full potential in real-world applications.

Data Availability Raw data that support the findings of this study are available from the corresponding author, upon reasonable request. The secondary data analysed during this study are from published sources, which are duly cited within the article.

Declarations

Conflict of interest No conflict of interest exist regarding the submitted work.

Open Access This article is licensed under a Creative Commons Attribution 4.0 International License, which permits use, sharing, adaptation, distribution and reproduction in any medium or format, as long as you give appropriate credit to the original author(s) and the source, provide a link to the Creative Commons licence, and indicate if changes were made. The images or other third party material in this article are included in the article's Creative Commons licence, unless indicated otherwise in a credit line to the material. If material is not included in the article's Creative Commons licence and your intended use is not permitted by statutory regulation or exceeds the permitted use, you will need to obtain permission directly from the copyright holder. To view a copy of this licence, visit http://creativecommons.org/licenses/by/4.0/.

References

1. Ding, L., Niu, L. Z., Su, Y., Yang, H. G., Liu, G. J., Gao, H. B., & Deng, Z. Q. (2022). Dynamic finite element modeling and simulation of soft robots. *Chinese Journal of Mechanical Engineering, 35*(1), 24. https://doi.org/10.1186/s10033-022-00701-8
2. Niu, L. Z., Ding, L., Zhang, S. J., Yang, H. G., Gao, H. B., Deng, Z. Q., Liu, G. J., & Hossain, M. (2023). Sospider: A bio-inspired multimodal untethered soft hexapod robot for planetary lava tube exploration. *Science China Technological Sciences, 66*(11), 3090–3106. https://doi.org/10.1007/s11431-023-2519-9
3. Chen, Y. F., Wang, H. Q., Helbling, E. F., Jafferis, N. T., Zufferey, R., Ong, A., Ma, K., Gravish, N., Chirarattananon, P., Kovac, M., & Wood, R. J. (2017). A biologically inspired, flapping-wing, hybrid aerial-aquatic microrobot. *Science Robotics* 2(11), eaao5619. https://doi.org/10.1126/scirobotics.aao5619
4. Li, Q., Li, H. Z., Shen, H., Yu, Y. G., He, H. R., Feng, X. C., Sun, Y., Mao, Z. Y., Chen, G. M., Tian, Z. J., Shen, L., Zheng, X. M., & Ji, A. H. (2023). An aerial-wall robotic insect that can land, climb, and take off from vertical surfaces. *Research, 6*, 0144. https://doi.org/10.34133/research.0144
5. Hassanalian, M., & Abdelkefi, A. (2017). Classifications, applications, and design challenges of drones: A review. *Progress in Aerospace Sciences, 91*, 99–131. https://doi.org/10.1016/j.paerosci.2017.04.003
6. Petricca, L., Ohlckers, P., & Grinde, C. (2011). Micro- and nano-air vehicles: State of the art. *International Journal of Aerospace Engineering, 2011*(1), 214549. https://doi.org/10.1155/2011/214549
7. Ellington, C. P. (1999). The novel aerodynamics of insect flight: Applications to micro-air vehicles. *Journal of Experimental Biology, 202*, 3439–3448. https://doi.org/10.1242/jeb.202.23.3439
8. Sachs, G. (2016). Comparison of power requirements: Flapping vs. fixed wing vehicles. *Aerospace, 3*(4), 31. https://doi.org/10.3390/aerospace3040031
9. Hawkes, E. W., & Lentink, D. (2016). Fruit fly scale robots can hover longer with flapping wings than with spinning wings. *Journal of The Royal Society Interface, 13*(123), 20160730. https://doi.org/10.1098/rsif.2016.0730
10. Zheng, L., Hedrick, T., & Mittal, R. (2013). A comparative study of the hovering efficiency of flapping and revolving wings. *Bioinspiration and Biomimetics, 8*(3), 036001. https://doi.org/10.1088/1748-3182/8/3/036001
11. Keennon, M., Klingebiel, K., Won, H., & Andriukov, A. (2012). Development of the nano hummingbird: A tailless flapping wing micro air vehicle. 50th AIAA Aerospace Sciences Meeting including the New Horizons Forum and Aerospace Exposition, Nashville, Tennessee, USA, 2012, 588. https://doi.org/10.2514/6.2012-588
12. Chechetka, S. A., Yu, Y., Tange, M., & Miyako, E. (2017). Materially engineered artificial pollinators. *Chem, 2*(2), 224–239. https://doi.org/10.1016/j.chempr.2017.01.008
13. Bomphrey, R. J., & Godoy-Diana, R. (2018). Insect and insect-inspired aerodynamics: Unsteadiness, structural mechanics and flight control. *Current Opinion in Insect Science, 30*, 26–32. https://doi.org/10.1016/j.cois.2018.08.003
14. Nachtigall, W. (2018). Mechanics and aerodynamics of flight. *Insect Flight,* 1–29. https://doi.org/10.1201/9781351073585
15. Vandenberghe, N., Zhang, J., & Childress, S. (2004). Symmetry breaking leads to forward flapping flight. *Journal of Fluid Mechanics, 506*, 147–155. https://doi.org/10.1017/S0022112004008468
16. Fitchett, B. K. (2007). Development and investigation of a flapping rotor for micro air vehicles. Ph.D. thesis, University of Maryland.
17. Guo, S. J., Yang, D. Q., Kummari, K. L., & Huang, Z. R. (2009). A smart material flapping wing micro rotorcraft. *17th ICCM International Conferences on Composite Materials,* Edinburgh, UK, 2009.
18. Guo, S. J., Li, D. C., & Wu, J. H. (2012). Theoretical and experimental study of a piezoelectric flapping wing rotor for micro aerial vehicle. *Aerospace Science and Technology, 23*(1), 429–438. https://doi.org/10.1016/j.ast.2011.10.002
19. Li, D. C., Guo, S. J., Di Matteo, N., & Yang, D. Q. (2011). Design, experiment and aerodynamic calculation of a flapping wing rotor micro aerial vehicle. *52nd AIAA/ASME/ASCE/AHS/ASC Structures, Structural Dynamics and Materials Conference,* Denver, Colorado, USA, 2011, 1–9. https://doi.org/10.2514/6.2011-1988.

20. Wu, J. H., Zhou, C., & Zhang, Y. L. (2012). A novel design in micro-air-vehicle: Flapping rotary wings. *Applied Mechanics and Materials, 232*, 189–193. https://doi.org/10.4028/www.scientific.net/AMM.232.189
21. Guo, S. J., Li, H., Zhou, C., Zhang, Y. L., He, Y., & Wu, J. H. (2018). Analysis and experiment of a bio-inspired flyable micro flapping wing rotor. *Aerospace Science and Technology, 79*, 506–517. https://doi.org/10.1016/j.ast.2018.06.009
22. Dong, X., Li, D. C., Xiang, J. W., & Wang, Z. Y. (2020). Design and experimental study of a new flapping wing rotor micro aerial vehicle. *Chinese Journal of Aeronautics, 33*(12), 3092–3099. https://doi.org/10.1016/j.cja.2020.04.024
23. Chen, S., Wang, L., He, Y. Y., Tong, M. B., Pan, Y. J., Ji, B., & Guo, S. J. (2022). Aerodynamic performance of a flyable flapping wing rotor with passive pitching angle variation. *IEEE Transactions on Industrial Electronics, 69*(9), 9176–9184. https://doi.org/10.1109/TIE.2021.3112964
24. Biewener, A. A., & Patek, S. N. (2018). *Animal locomotion* (2nd ed., pp. 1–223). Oxford University Press. https://doi.org/10.1093/oso/9780198743156.001.0001
25. Alexander, D. E. (2002). *Nature's flyers: Birds, insects, and the biomechanics of flight*. Johns Hopkins University Press.
26. Sane, S. P. (2003). The aerodynamics of insect flight. *Journal of Experimental Biology, 206*(23), 4191–4208. https://doi.org/10.1242/jeb.00663
27. Li, H., Guo, S. J., Zhang, Y. L., Zhou, C., & Wu, J. H. (2017). Unsteady aerodynamic and optimal kinematic analysis of a micro flapping wing rotor. *Aerospace Science and Technology, 63*, 167–178. https://doi.org/10.1016/j.ast.2016.12.025
28. Ward, T. A., Rezadad, M., Fearday, C. J., & Viyapuri, R. (2015). A review of biomimetic air vehicle research: 1984–2014. *International Journal of Micro Air Vehicles, 7*(3), 375–394. https://doi.org/10.1260/1756-8293.7.3.375
29. Salami, E., Ward, T. A., & Montazer, E. (2019). A review of aerodynamic studies on dragonfly flight. *Proceedings of the Institution of Mechanical Engineers, Part C: Journal of Mechanical Engineering Science, 233*(18), 6519–6537. https://doi.org/10.1177/0954406219861133
30. Wu, J. H., Zhou, C., & Zhang, Y. L. (2016). Aerodynamic power efficiency comparison of various micro-Air-vehicle layouts in hovering flight. *AIAA Journal, 55*(4), 1265–1278. https://doi.org/10.2514/1.J055221
31. Wu, J. H., Qiu, J., & Zhang, Y. L. (2017). Automated kinematics measurement and aerodynamics of a bioinspired flapping rotary wing. *Journal of Bionic Engineering, 14*(4), 726–737. https://doi.org/10.1016/S1672-6529(16)60438-9
32. Zhou, C., Wu, J. H., Guo, S. J., & Li, D. C. (2014). Experimental study on the lift generated by a flapping rotary wing applied in a micro air vehicle. *Proceedings of the Institution of Mechanical Engineers, Part G: Journal of Aerospace Engineering, 228*(11), 2083–2093. https://doi.org/10.1177/0954410013512761
33. Chen, S., Wang, L., Guo, S. J., Zhao, C. S., & Tong, M. B. (2020). A bio-inspired flappingwing rotor of variant frequency driven by ultrasonic motor. *Applied Sciences, 10*(1), 1–21. https://doi.org/10.3390/app10010412
34. Chen, F., Wu, J. H., Zhou, C., & Zhang, Y. L. (2013). An automatical matching method applied in kinematics measurement for the flapping rotary wing. *Applied Mechanics and Materials, 459*, 119–124. https://doi.org/10.4028/www.scientific.net/AMM.459.119
35. Zhu, Z. G., Zhao, J. T., He, Y. Y., Guo, S. J, Chen, S., & Ji, B. (2022). Aerodynamic analysis of insect-like flapping wings in fan-sweep and parallel motions with the slit effect. *Biomimetic Intelligence and Robotics, 2*, 100046. https://doi.org/10.1016/j.birob.2022.100046
36. Wang, Z. J. (2004). The role of drag in insect hovering. *Journal of Experimental Biology, 207*(23), 4147–4155. https://doi.org/10.1242/jeb.01239
37. Phan, H. V., & Park, H. C. (2019). Insect-inspired, tailless, hover-capable flapping-wing robots: Recent progress, challenges, and future directions. *Progress in Aerospace Sciences, 111*, 100573. https://doi.org/10.1016/j.paerosci.2019.100573
38. Li, H., & Guo, S. J. (2018). Aerodynamic efficiency of a bioinspired flapping wing rotor at low Reynolds number. *Royal Society Open Science, 5*(3), 171307. https://doi.org/10.1098/rsos.171307
39. Wang, D., Wu, J. H., & Zhang, Y. L. (2013). Aerodynamics on flapping rotary wing in low reynolds number. *2013 International powered lift conference,* Los Angeles, CA, USA, 2013. https://doi.org/10.2514/6.2013-4382
40. Wu, J. H., Wang, D., & Zhang, Y. H. (2015). Aerodynamic analysis of a flapping rotary wing at a low Reynolds number. *AIAA Journal, 53*(10), 2951–2966. https://doi.org/10.2514/1.J053845
41. Chen, S., Li, H., Guo, S. J., Tong, M., & Ji, B. (2018). Unsteady aerodynamic model of flexible flapping wing. *Aerospace Science and Technology, 80*, 354–367. https://doi.org/10.1016/j.ast.2018.07.017
42. Zhou, C., Zhang, Y. L., & Wu, J. H. (2018). Unsteady aerodynamic forces and power consumption of a micro flapping rotary wing in hovering flight. *Journal of Bionic Engineering, 15*(2), 298–312. https://doi.org/10.1007/s42235-018-0023-y
43. Wang, D., Wu, J. H., & Zhang, Y. L. (2018). Effects of geometric parameters on flapping rotary wings at low Reynolds numbers. *AIAA Journal, 56*(4), 1372–1387. https://doi.org/10.2514/1.J055994
44. Wu, J. H., Yan, H., Zhou, C., & Zhang, Y. L. (2021). Unsteady aerodynamics of a micro flapping rotary wing in forward flight. *Aerospace Science and Technology, 111*, 106530. https://doi.org/10.1016/j.ast.2021.106530
45. Chen, L., Yan, W., & Wu, J. H. (2015). Experimental validation on lift increment of a flapping rotary wing with boring-hole design. *Procedia Engineering, 99*, 1543–1547. https://doi.org/10.1016/j.proeng.2014.12.706
46. Ellington, C. P. (1984). The aerodynamics of hovering insect flight. VI. Lift and power requirements. *Philosophical Transactions of the Royal Society of London B, Biological Sciences, 305*(1122), 145–181. https://doi.org/10.1098/rstb.1984.0054
47. Chin, D. D., & Lentink, D. (2016). Flapping wing aerodynamics: From insects to vertebrates. *Journal of Experimental Biology, 219*(7), 920–932. https://doi.org/10.1242/jeb.042317
48. Triantafyllou, G. S., Triantafyllou, M. S., & Grosenbaugh, M. A. (1993). Optimal thrust development in oscillating foils with application to fish propulsion. *Journal of Fluids and Structures, 7*(2), 205–224. https://doi.org/10.1006/jfls.1993.1012
49. Taylor, G. K., Nudds, R. L., & Thomas, A. L. R. (2003). Flying and swimming animals cruise at a Strouhal number tuned for high power efficiency. *Nature, 425*, 707–711. https://doi.org/10.1038/nature02000
50. Kruyt, J. W., Quicazán-Rubio, E. M., Van Heijst, G. F., Altshuler, D. L., & Lentink, D. (2014). Hummingbird wing efficacy depends on aspect ratio and compares with helicopter rotors. *Journal of The Royal Society Interface, 11*, 20140585. https://doi.org/10.1098/rsif.2014.0585
51. Lentink, D., & Dickinson, M. H. (2009). Rotational accelerations stabilize leading edge vortices on revolving fly wings. *Journal of Experimental Biology, 212*(16), 2705–2719. https://doi.org/10.1242/jeb.022269
52. U.S. Department of Transportation, Federal Aviation Administration. (2019). Helicopter Flying Handbook (FAA-H-8083-21B) (pp. 208). U.S. Department of Transportation, Washington, DC.
53. Meng, X. G., & Sun, M. (2011). Aerodynamic effects of corrugation in flapping insect wings in forward flight. *Journal of Bionic*

Engineering, 8(2), 140–150. https://doi.org/10.1016/S1672-6529(11)60015-2
54. Dickson, W. B., & Dickinson, M. H. (2004). The effect of advance ratio on the aerodynamics of revolving wings. *Journal of Experimental Biology, 207*(24), 4269–4281. https://doi.org/10.1242/jeb.01266
55. Nagai, H., & Isogai, K. (2011). Effects of flapping wing kinematics on hovering and forward flight aerodynamics. *AIAA Journal, 49*(8), 1750–1762. https://doi.org/10.2514/1.J050968
56. Wu, J. H., Chen, L., Zhou, C., Hsu, S. J., & Cheng, B. (2019). Aerodynamics of a flapping-perturbed revolving wing. *AIAA Journal, 9*, 3728–3743. https://doi.org/10.2514/1.J056584
57. Wang, H., Zeng, L. J., Liu, H., & Yin, C. Y. (2003). Measuring wing kinematics, flight trajectory and body attitude during forward flight and turning maneuvers in dragonflies. *Journal of Experimental Biology, 206*(4), 745–757. https://doi.org/10.1242/jeb.00183
58. Du, G., & Sun, M. (2008). Effects of unsteady deformation of flapping wing on its aerodynamic forces. *Applied Mathematics and Mechanics, 29*(6), 731–743. https://doi.org/10.1007/s10483-008-0605-9
59. Shao, H. Y., Li, D. C., Kan, Z., Li, H. D., Yuan, D., & Xiang, J. W. (2021). Influence of wing camber on aerodynamic performance of flapping wing rotor. *Aerospace Science and Technology, 113*, 106732. https://doi.org/10.1016/j.ast.2021.106732
60. Li, G. J., Liu, N. S., & Lu, X. Y. (2014). Dynamic performance and wake structure of flapping plates with different shapes. *Acta Mechanica Sinica, 30*, 800–808. https://doi.org/10.1007/s10409-014-0112-z
61. Gao, G. L., Song, B. F., Wang, L. G., & Ding, X. (2010). Study of opening holes on the wing of flapping-wing MAV and its effect on aerodynamic characteristic. *Shiyan Liuti Lixue/Journal of Experiment in Fluid Mechanics, 24*(5), 70–73.
62. Chen, L., Zhou, Y., Zhou, C., & Wu, J. H. (2022). Effects of bore-hole design on the aerodynamics of a flapping rotary wing in forward flight. *Aerospace Science and Technology, 127*, 107671. https://doi.org/10.1016/j.ast.2022.107671
63. Chen, L., Wang, L. Y., & Wang, Y. Q. (2022). Efficient fluid–structure interaction model for twistable flapping rotary wings. *AIAA Journal, 12*, 6665–6679. https://doi.org/10.2514/1.J061940
64. Wang, L. Y., Chen, L., & Wang, Y. Q. (2023). Optimal stiffness design of a twistable flapping rotary wing in hovering flight. *Proceedings of 2022 International Conference on Autonomous Unmanned Systems (ICAUS 2022),* Singapore, 2022, 358–367.
65. He, Y. Y., Zhang, H., & Wang, Q. C. (2023). Effect of stiffness and wingtip shape on aerodynamic lift and efficiency of flapping wing rotors. *Acta Aeronautica et Astronautica Sinica, 44*(12), 127779. In Chinese.
66. Guan, Z., & Yu, Y. (2014). Aerodynamic mechanism of forces generated by twisting model-wing in bat flapping flight. *Applied Mathematics and Mechanics, 12*, 1607–1618. https://doi.org/10.1007/s10483-014-1882-6
67. Truong, T. Q., Phan, V. H., Park, H. C., & Ko, J. H. (2013). Effect of wing twisting on aerodynamic performance of flapping wing system. *AIAA Journal, 51*(7), 1612–1620. https://doi.org/10.2514/1.J051831
68. Ghommem, M., Hajj, M. R., Beran, P. S., & Puri, I. K. (2014). Role of wing morphing in thrust generation. *Theoretical and Applied Mechanics Letters, 3*, 032003. https://doi.org/10.1063/2.1403203
69. Alexander, R. M., & Bennet-Clark, H. C. (1977). Storage of elastic strain energy in muscle and other tissues. *Nature, 265*, 114–117. https://doi.org/10.1038/265114a0
70. Steltz, E., Avadhanula, S., & Fearing, R. S. (2007). High lift force with 275 hz wing beat in mfi. *2007 IEEE/RSJ International Conference on Intelligent Robots and Systems,* San Diego, CA, USA, 2007, 3987–399. https://doi.org/10.1109/IROS.2007.4399068
71. Tantanawat, T., & Kota, S. (2007). Design of compliant mechanisms for minimizing input power in dynamic applications. *Journal of Mechanical Design, 10*, 1064–1075. https://doi.org/10.1115/1.2756086
72. Baek, S., Ma, K., & Fearing, R. (2009). Efficient resonant drive of flapping-wing robots. *2009 IEEE/RSJ International Conference on Intelligent Robots and Systems,* St. Louis, MO, USA, 2009, 2854–2860. https://doi.org/10.1109/IROS.2009.5354725
73. Yi, S., Li, D. C., Jiang, J. Q., Xiang, J. W., & Xu, W. (2017). Design and experimental study of a new flapping wing rotor micro aerial vehicle. *2017 IEEE International Conference on Unmanned Systems (ICUS),* Beijing, China, 2017, 29–33. https://doi.org/10.1109/ICUS.2017.8278312
74. Dong, X., Wang, Z. Y., Liu, F. Y., Li, S., Fei, F., Li, D. C., & Tu, Z. (2022). Visual-inertial cross fusion: A fast and accurate state estimation framework for micro flapping wing rotors. *Drones, 6*(4), 1–18. https://doi.org/10.3390/drones6040090
75. Chen, L., Yang, F. L., & Wang, Y. Q. (2022). Analysis of nonlinear aerodynamic performance and passive deformation of a flexible flapping wing in hover flight. *Journal of Fluids and Structures, 108*, 10345. https://doi.org/10.1016/j.jfluidstructs.2021.103458
76. Karasek, M., Muijres, F. T., Wagter, C. D., Remes, B. D., & De Croon, G. C. (2018). A tailless aerial robotic flapper reveals that flies use torque coupling in rapid banked turns. *Science*, 361, 1089–1094. https://doi.org/10.1126/science.aat0350
77. Coleman, D., & Benedict, M. (2015). Design, development and flight-testing of a robotic hummingbird. *AHS 71st Annual Forum,* Virginia Beach, Virginia, USA, 2015, 5–7.
78. Roshanbin, A., Altartouri, H., Karásek, M., & Preumont, A. (2017). COLIBRI: A hovering flapping twin-wing robot. *International Journal of Micro Air Vehicles, 9*(4), 270–282. https://doi.org/10.1177/1756829317695563
79. Tu, Z., Fei, F., & Deng, X. Y. (2020). Untethered flight of an at-scale dual-motor hummingbird robot with bio-inspired decoupled wings. *IEEE Robotics and Automation Letters, 5*(3), 4194–4201. https://doi.org/10.1109/LRA.2020.2974717
80. Nguyen, Q. V., & Chan, W. L. (2019). Development and flight performance of a biological-inspired tailless flapping wing micro air vehicle with wing stroke plane modulation. *Bioinspiration & Biomimetics, 14*(1), 016015. https://doi.org/10.1088/1748-3190/aaefa0
81. Azhar, M., Campolo, D., Lau, G K., Hines, L., & Sitti, M. (2013). Flapping wings via direct-driving by dc motors. *2013 IEEE International Conference on Robotics and Automation,* Karlsruhe, Germany, 2013, 1397–1402. https://doi.org/10.1109/ICRA.2013.6630753
82. Leys, F., Reynaerts, D., & Vandepitte, D. (2016). Outperforming hummingbirds' load-lifting capability with a lightweight hummingbird-like flapping-wing mechanism. *Biology Open, 5*(8), 1052–1060. https://doi.org/10.1242/bio.014357
83. Leys, F., Vandepitte, D., & Reynaerts, D. (2015). Design of a flapping wing micro air vehicle, based on the rufous hummingbird. *2015 IEEE International Conference on Robotics and Biomimetics (ROBIO),* Zhuhai, China, 2015, 1266–1271. https://doi.org/10.1109/ROBIO.2015.7418945
84. Helbling, F. E., & Wood, R. J. (2018). A review of propulsion, power, and control architectures for insect-scale flapping-wing vehicles. *Applied Mechanics Reviews, 70*(1), 010801. https://doi.org/10.1115/1.4038795

Publisher's Note Springer Nature remains neutral with regard to jurisdictional claims in published maps and institutional affiliations.

https://dspace.org/

Research progress on bio-inspired flapping-wing rotor micro aerial vehicle development

Pan, Yingjun; Guo, Shijun; Huang, Xun

2024-07-01
Springer
https://doi.org/10.1007/s42235-024-00521-7
Pan Y, Guo S, Huang X. (2024) Research progress on bio-inspired flapping-wing rotor micro aerial vehicle development. Journal of Bionic Engineering, Volume 21, July 2024, pp. 1621-1643

Downloaded from a DSpace repository. https://dspace.org/